Quaternary Science Reviews 288 (2022) 107577

Contents lists available at ScienceDirect

Quaternary Science Reviews

journal homepage: www.elsevier.com/locate/quascirev

Human occupation of the Kimberley coast of northwest Australia 50,000 years ago

Kasih Norman [a, b, *], Ceri Shipton [c, d], Sue O'Connor [d, e], Wudugu Malanali [f], Peter Collins [g], Rachel Wood [d, h, i], Wanchese M. Saktura [b], Richard G. Roberts [a, b], Zenobia Jacobs [a, b]

[a] Centre for Archaeological Science, School of Earth, Atmospheric and Life Sciences, University of Wollongong, Wollongong, New South Wales, 2522, Australia
[b] ARC Centre of Excellence for Australian Biodiversity and Heritage, University of Wollongong, Wollongong, New South Wales, 2522, Australia
[c] Institute of Archaeology, University College London, London, WC1H 0PY, UK
[d] ARC Centre of Excellence for Australian Biodiversity and Heritage, Australian National University, Canberra, Australian Capital Territory, 2601, Australia
[e] Department of Archaeology and Natural History, School of Culture, History and Language, Australian National University, Canberra, Australian Capital Territory, 2601, Australia
[f] Arraluli Clan, PO Box 4180, Myaree, 6960, Australia
[g] Arraluli Aboriginal Association, PO Box 4180, Myaree, 6960, Australia
[h] School of Archaeology and Anthropology, Australian National University, Canberra, Australian Capital Territory, 2601, Australia
[i] Research School of Earth Sciences, Australian National University, Canberra, Australian Capital Territory, 2601, Australia

ARTICLE INFO

Article history:
Received 24 March 2022
Received in revised form
17 May 2022
Accepted 17 May 2022
Available online 13 June 2022

Handling Editor: Donatella Magri

Keywords:
Widgingarri 1
Western Australia
Stone artefacts
Radiocarbon dating
Optical dating
Single-grain OSL
Northern Sahul

ABSTRACT

The peopling of Sahul (the combined landmass of New Guinea and Australia) is a topic of much debate. The Kimberley region of Western Australia holds many of Australia's oldest known archaeological sites. Here, we review the chronological and archaeological data available for the Kimberley from early Marine Isotope Stage 3 to the present, linking episodes of site establishment and the appearance of new technologies with periods of climatic and sea-level change. We report optical ages showing human occupation of Widgingarri 1, a rockshelter located on the Kimberley coast of northwest Australia, as early as 50,000 years ago, when the site was located more than 100 km from the Late Pleistocene coastline. We also present the first detailed analysis of the stone artefacts, including flakes from ground stone axes, grinding stones and ground haematite recovered from the deepest excavated layer. The high proportion of flakes from ground axe production and resharpening in the earliest occupation phase emphasises the importance of this complex technology in the first peopling of northern Sahul. Artefact analyses indicate changes in settlement patterns through time, with an increase in mobility in the terminal Pleistocene and a shift to lower mobility during the late Holocene. The optical ages for Widgingarri 1 mean that the Kimberley now contains the greatest number of sites in Sahul with earliest occupation dated to more than 46,000 years ago, overlapping with the time of initial occupation of sites in other regions across the continent.

1. Introduction

The Kimberley is a large region in northwest Australia with a rich cultural record that includes some of the oldest known archaeological sites in Sahul (the combined landmass of Australia and New Guinea at times of lower sea level) (Wood et al., 2016; Maloney et al., 2018; Veth et al., 2019). It is considered a potential entry point for the peopling of Australia via the 'southern gateway' seafaring route. Recent migration models (Bird et al., 2018; Kealy et al., 2018; Norman et al., 2018; Bird et al., 2019) and genetic studies (Nagle et al., 2017; Yuen et al., 2019; Pedro et al., 2020) suggest the early peopling of Sahul potentially occurred through the Bird's Head of New Guinea (or northern gateway) and/or the Australian Northwest Shelf (or southern gateway) (Fig. 1A). The Kimberley is located in a strategic position directly adjacent to the now-submerged Northwest Shelf, a large region of the Australian continental shelf that may have supported a substantial human

* Corresponding author. Centre for Archaeological Science, School of Earth, Atmospheric and Life Sciences, University of Wollongong, Wollongong, New South Wales, 2522, Australia.
E-mail address: kbn686@uowmail.edu.au (K. Norman).

https://doi.org/10.1016/j.quascirev.2022.107577

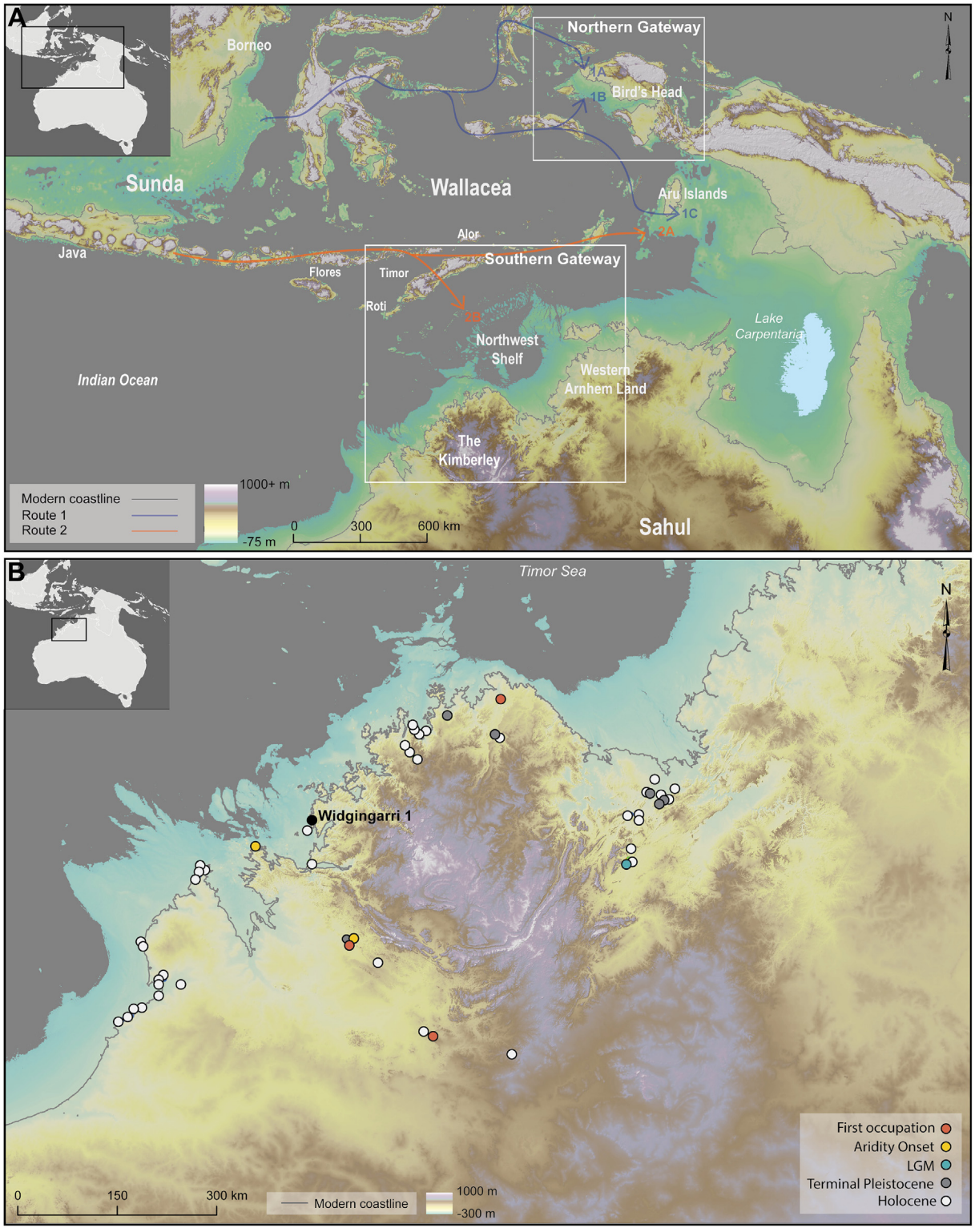

Fig. 1. **A**, Wallacea and northern Sahul with the northern and southern routes (Birdsell, 1977) shown by arrows and numbered accordingly. Gateway regions are delineated by white boxes. The Northwest Shelf of Sahul extends below the modern coastline (shown in grey), with the Kimberley forming part of Australia's southern gateway. **B**, The Kimberley region, showing the spatial and temporal distribution of human occupation sites, with the location of Widgingarri 1 shown. The legend colours correspond to the five site establishment pulses discussed in text. (For interpretation of the references to colour in this figure legend, the reader is referred to the Web version of this article.)

population in the Late Pleistocene (Bradshaw et al., 2021) (Fig. 1A). The Kimberley is, therefore, an important region for ground-truthing migration and demographic models, as well as understanding early Aboriginal lifeways.

It should also be noted that the current direct descendants of the people whose occupation evidence is being studied, and whose consistency of localised habitation has been supported by other scientific studies such as those looking at DNA of Australian

Aboriginal peoples, have their own cosmology, views and histories that consider what we term as occupation, presence or peopling. These are sensitive matters when discussing migration theories, but are not necessarily irreconcilable with local Aboriginal histories and cosmology, which should also be considered in developing and propagating these hypotheses.

In this paper, we first undertake an analysis and synthesis of chronological and archaeological data for the Kimberley, and outline distinct patterns in landscape use and technological and cultural responses to climatic and sea-level change from Marine Isotope Stage 3 (MIS 3) to the present. We then report new information for the human occupation site of Widgingarri 1, located on the western coastal margin of the region, including the first detailed analysis of the stone artefact assemblage from Square AA. For the same excavation square, we provide single-grain optical age estimates for four sediment samples collected in 1993 to determine the stratigraphic integrity and age of the artefact-bearing sedimentary deposits, as well as new radiocarbon ages for previously dated baler shell and charcoal. We conclude by reassessing the stratigraphic integrity and age of the deposits encasing the artefacts, and re-position Widgingarri 1 in the broader archaeological record of the Kimberley. Finally, we present a suite of new Bayesian age models for the oldest occupation sites across Sahul and contextualise Widgingarri 1 and the Kimberley within the broader continental pattern of first peopling.

2. Landscape use and cultural innovation in the Kimberley, MIS 3 to present

The Kimberley is bordered by the Timor Sea and the Indian Ocean to the north and west, and the vast Australian arid zone to the south (Fig. 1B). The region encompasses more than 400,000 km^2 of land area, has a tropical monsoon climate, and is predominantly comprised of dissected sandstone plateaus that are well-suited to the formation of rockshelters.

2.1. Site distribution and time of establishment

Sixty-three dated archaeological sites are known from the Kimberley (Table S1), including numerous dated examples of rock art. Sites are predominantly distributed along the modern coastal fringe, with a smaller number of dated inland sites located around the periphery of the region (Fig. 1B). A notable spatial gap occurs in dated sites across the plateaus, potentially due to a lack of datable deposits in rockshelters in this area (Veth et al., 2019). Site numbers are low (n = 13) across the Kimberley prior to the mid-Holocene (8.2–4.2 ka), with all known sites located well inland prior to the formation of the modern coastline. Once sites were initially established, many appear to continue to have been visited, often into the European contact period.

Site establishment (first use of a site) occurs in five main pulses (Figs. 1B and 2A) across the Kimberley, each with a slightly different geographic distribution. To be clear, we are referring only to pulses in site establishment and not to occupational intensity. Each new pulse represents a cumulative increase in the total number of sites occupied by people. Table S1 presents a list of all 63 sites, divided into five pulses of site establishment, together with information about site type and age estimates for their earliest occupation (see Supplementary Information).

The first and earliest pulse in site establishment occurs between ~49 and 45 thousand years ago (ka) on both the northern and southern margins of the region (Figs. 1B and 2A, orange; Table S1). In the north, early occupation at Minjiwarra is very sparse (Veth et al., 2019), while the records at both Carpenter's Gap 1 (CG1) and Riwi in the south show intermittent low-intensity occupation following first occupation (Wood et al., 2016; Maloney et al., 2018; Balme et al., 2019). The second pulse in site establishment occurs approximately 17,000 years later, between ~32 and 30 ka (Figs. 1B and 2A, yellow; Table S1), coinciding with a period of heightened aridity between 35 and 29 ka at the end of MIS 3 (Kemp et al., 2019). Initial occupation at Carpenter's Gap 3 (CG3), Koolan Rockshelter and Widgingarri 1, which are located in the southern and western Kimberley, has been dated to this time (O'Connor, 1999, O' Connor et al., 2014).

The third pulse (Figs. 1B and 2A, green; Table S1) occurs during the height of the Last Glacial Maximum (LGM), with occupation beginning at Miriwun in the Keep River region of the eastern Kimberley (Dortch and Roberts, 1996). The fourth pulse (Figs. 1B and 2A, grey; Table S1) occurs in the terminal Pleistocene, appearing over a wider geographic area. This period contains two sub-pulses, which occur at the end of the LGM (19–17 ka), and just prior to the onset of the Holocene (14–13 ka). Site types become more varied in this fourth pulse, including dated figurative rock art sites (DR015_10 and KERC), a dated cupule (Jinmium KR24), and three new occupation sites (Karlinga 3, Djuru/Windjana Gorge Water Tank Shelter and Goorurarmum-1) (Roberts et al., 1997; Watchman et al., 2000; Ward et al., 2005; Ward et al., 2006; O'Connor et al., 2008; Maloney et al., 2016; Finch et al., 2021).

A hiatus in the establishment of new sites occurs during the early Holocene (n = 1), although occupation continues at numerous sites established previously. Site numbers increase substantially in the mid-to-late Holocene, with 50 new sites established during this fifth pulse (Figs. 1B and 2A, white; Table S1). This increase occurs in already-occupied regions, as well as along the newly formed coastline. The fifth pulse of site establishment also includes the large-scale appearance of anthropogenic shell middens for the first time (Fig. 2D).

We note that the absence of archaeological evidence for initial site occupation between pulses does not necessarily imply that new sites were not occupied during these periods. The patterns observed here may instead represent time gaps in the preserved sedimentary record and/or spatial and temporal gaps in the archaeological record of the Kimberley more broadly.

2.2. Artefact assemblages and technologies

The Kimberley has some of the earliest examples of complex material culture and symbolic cultural behaviour in Sahul, including one of the largest and richest concentrations of rock art found worldwide (Aubert, 2012). Some of the earliest examples of ground stone axe technology in Sahul are found in the southern Kimberley (Hiscock et al., 2016). This complex technology appears from first occupation in stratigraphic unit (SU8) at CG1 (Fig. 2E), deposited ~50–40 ka, and is present at other sites in at least one assemblage in each of the establishment pulses, except during the terminal Pleistocene (Fig. 1B, grey) (Dortch and Roberts, 1996; O'Connor et al., 2014; Maloney et al., 2018; Veth et al., 2019). The earliest known worked bone technology in Sahul takes the form of a personal ornament found in the same cultural layer (SU8) as the earliest axe technology at CG1 (Fig. 2E) (Langley et al., 2016). Worked bone artefacts are also found in the lowest cultural unit (SU11) at Riwi (~45–42 ka), with this technology occurring throughout the sequence (Balme et al., 2019, Langley et al., 2021).

Symbolic behaviour, evidenced by the presence of red ochre, appears very early in the southern Kimberley (Fig. 2E), including in SU11 at Riwi, SU7 at CG1 (~40–30 ka) and ochre-stained roof fall at CG1 dated to ~40 ka (O'Connor et al., 2001, Wood et al., 2016; Maloney et al., 2018; Balme et al., 2019). Ochre is also present in the lowest cultural levels (and throughout the archaeological deposits) of sites in the eastern Kimberley with initial occupation dating to

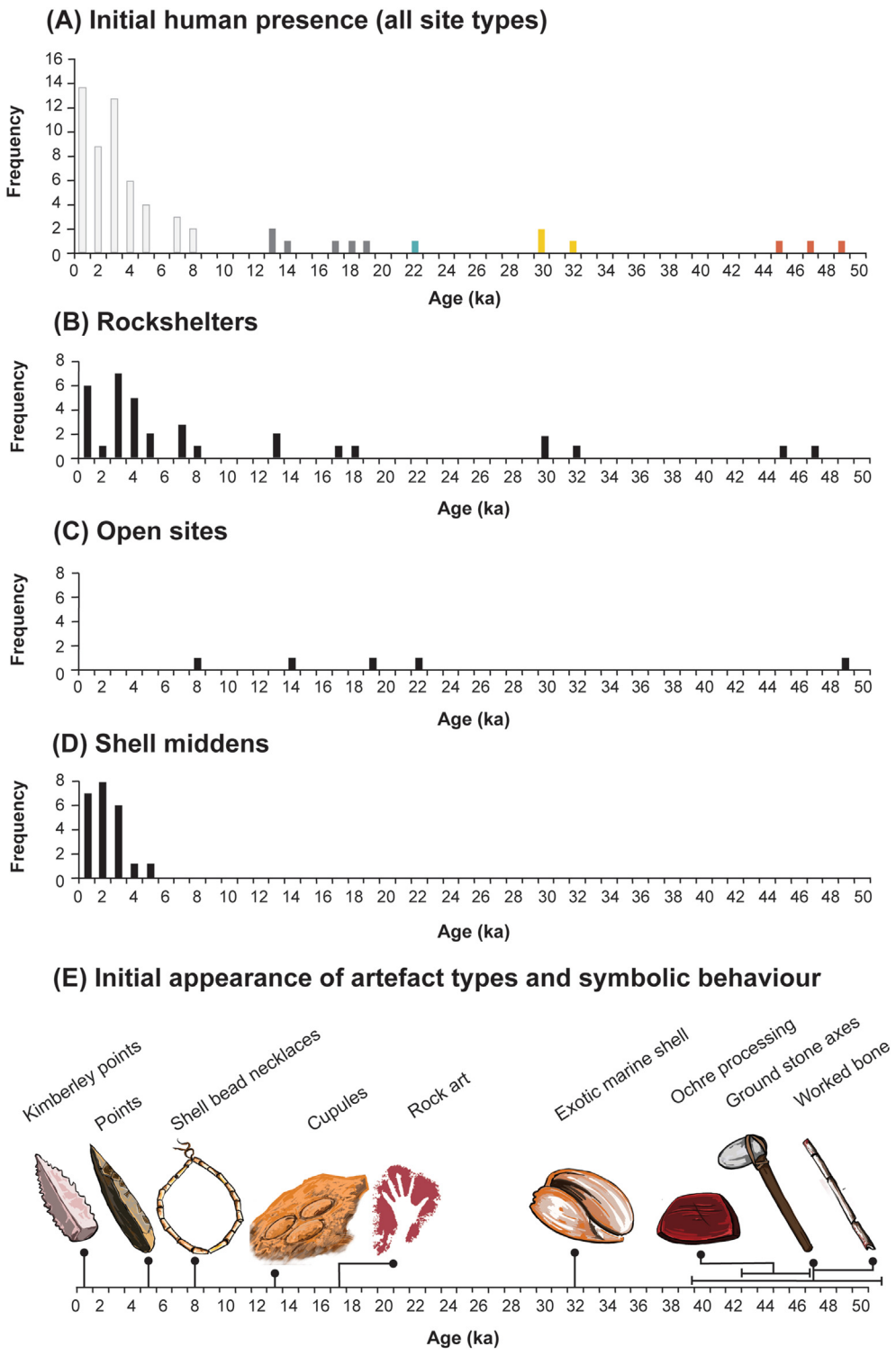

Fig. 2. **A**, Frequency plot of all site types showing initial onset of site occupation through time. Colours cross-reference to Fig. 1B. Age estimates are provided in Table S1 and sourced from the SahulArch collection (Saktura et al., 2021a; 2021b; Cohen et al., 2021) of the OCTOPUS v.2 database (Codilean et al., 2021). **B**–**D**, Frequency plots of single site types showing onset of occupation through time. **E**, Initial appearance of artefact types and symbolic behaviour. Age estimates indicated are either approximate for the region (e.g., points), represent direct dates (such as for shell artefacts), or represent the Bayesian modelled range (95.4% confidence interval) for the occupation phase from which the artefacts derive (e.g., ochre, ground stone axes). (For interpretation of the references to colour in this figure legend, the reader is referred to the Web version of this article.)

the terminal Pleistocene (Karlinga-3 and Goorurarmum-1) (Ward et al., 2006).

Archaeological sites in the second pulse of occupation in the southeast Kimberley (Figs. 1B and 2A, yellow) have some of the earliest evidence for the use of exotic marine shell, such as pearl (*Pintada* sp.) and baler shell (*Melo amphora*) (Fig. 2E) (O'Connor, 1999). These sites are located on the edge of the now-submerged coastal plain that formed part of the Northwest Shelf, indicating

that people visited the Late Pleistocene coast. These shells were highly valued items and were widely traded into the interior of the continent (Balme et al., 2017; Akerman, 2018).

The fourth pulse (Figs. 1B and 2A, grey) includes the earliest examples of figurative art yet found in Australia, with anthropomorphic and naturalistic animal motifs dated to ~17 ka or possibly earlier (Fig. 2E; Table S1) (Roberts et al., 1997; Finch et al., 2021). In the east Kimberley, examples of enigmatic 'cupule' pecked rock engravings have minimum ages from the terminal Pleistocene to the late Holocene (Watchman et al., 2000). In the south Kimberley, scaphopod (tusk shell) beads are found in archaeological sites from ~8 ka through to the late Holocene (O'Connor et al., 2014; Maloney et al., 2016, Balme et al., 2017; Maloney, et al., 2018). Their presence indicates extensive trade networks with the coast that existed throughout this period, and provides unambiguous evidence for personal adornment in the early Holocene (Balme et al., 2017).

During the mid-to-late Holocene, new lithic technologies emerged in the Kimberley, including point and tula adze technology (Fig. 2E) (Maloney et al., 2014; Maloney and Dilkes-Hall, 2020). Points first appear at ~5 ka at multiple sites in the southern Kimberley (Maloney et al., 2014, 2017, 2018), with a slightly later appearance in east Kimberley assemblages (Keep River region), ~3–2.5 ka (Ward et al., 2005; Ward et al., 2006; Moore et al., 2020). Tulas appear in the southern Kimberley by ~2.7 ka, likely spreading west from the arid zone (Maloney and Dilkes-Hall, 2020). The earliest examples of pressure-flaked Kimberley points date to ~1 ka (Maloney et al., 2014), with this distinctive technology originating in the Kimberley region.

Current evidence suggests the Kimberley was initially occupied at low density, with occupation into new areas accompanying each pulse in site establishment. These pulses were typically tied to periods of climatic change, sea-level change, or both. A major increase in site numbers only occurred during the mid-to-late Holocene, along with the first appearance of shell middens. While occupation of many sites appears to have occurred episodically, the archaeological record of the Kimberley indicates permanent occupation of the region from the time of initial evidence of peopling (see also Veth et al., 2021). The terminal Pleistocene and the Holocene were periods of technological innovation and flourishing symbolic expression (Fig. 2E). Worked bone artefacts and rock art appear earlier in the Kimberley than elsewhere in Sahul, suggesting the region was an important zone of early cultural innovation. Nonetheless, the number of Pleistocene occupation sites presently known in the Kimberley is small, with the majority of sites dating to the mid-to-late Holocene, and large areas of the region remain archaeologically unknown.

3. Widgingarri 1 rockshelter

A site that can potentially make further contributions to our understanding of early occupation and lifestyles in the Kimberley is Widgingarri 1 rockshelter. Although now only 2 km from the coast, Widgingarri 1 was located as far as 100 km inland from the Late Pleistocene coastline. Published radiocarbon ages suggested occupation since the Late Pleistocene (O'Connor, 1999), but significant radiocarbon age inversions obtained using a variety of material types have raised questions about the antiquity and stratigraphic integrity of the deposit. Exotic marine shell fragments from the site gave measured radiocarbon ages of 18.9 ± 1.8 (ANU/AMS 5–10) and 28.1 ± 0.6 ka BP (R-11795), which correspond to calibrated age ranges (at the 95.4% confidence interval) of 18.3–27.3 and 30.2–33.0 cal ka BP, respectively (Table 1). A modern age was obtained from charcoal deriving from the same spit as the lowest shell sample, while the apatite fraction of bone fragments from the underlying layer gave early Holocene ages (O'Connor, 1999).

Inverted ages may result from post-depositional disturbance at a site and/or from the types of materials and sample pretreatments used for radiocarbon dating. Issues can include chemical contamination of the sample by modern carbon, and downward displacement of modern humic acids precipitating around inorganic matter and being mistaken for charcoal, as is suspected to have occurred at Widgingarri 1 (O'Connor, 1999). Radiocarbon dating of bone apatite usually underestimates the true age of a sample, because it is difficult to separate contaminating carbonate from the low concentration of endogenous carbonate in the bone mineral (Zazzo and Saliège, 2011; Storm et al., 2013). The radiocarbon ages obtained for samples of carbonate-encrusted bone from the lowest stratigraphic unit of Widgingarri 1 (Table 1) should, therefore, be regarded as unreliable.

3.1. Environmental context

Widgingarri 1 is a moderate-sized sandstone rockshelter (approximately 9 m deep and 14 m wide at its maximum extent) with an ashy floor and impressive rock art panels on the sloping ceiling. The site lies in the Prince Regent Plateau sub-province, which forms part of the Kimberley Basin and consists primarily of sedimentary and volcanic rocks, and has a northeast-facing aspect. The rockshelter is set into the exposed rocky substrate, and looks out over a broad and shallow valley containing many species of edible plants. The ceiling is low (<2 m) and slopes to the rear of the rockshelter, though in the past the lower floor height would have provided standing room throughout much of the shelter (Fig. 3). The archaeological potential of Widgingarri 1 was initially identified during extensive field surveys undertaken in 1984 with senior traditional owners of the Worrora, Umiida, and Yawjibaya Aboriginal people.

The environmental context of the Kimberley during MIS 3 (57–29 ka) through to the early Holocene (11.7–8.2 ka) was very different to that found today, because lowered sea level exposed a large extent of the now-drowned Northwest Shelf (Williams et al., 2018). Over this time interval, a broad and flat coastal plain extended up to ~100 km west from the site before reaching the coast (Fig. 1B). To the east lay the dissected sandstone plateaus of the central Kimberley. From the mid-Holocene (8.2–4.2 ka) to the present day, the site has been ~2 km from the modern coastline (Williams et al., 2018).

While the Kimberley experienced wetter conditions through much of MIS 3, the region experienced a drier climate between 35 and 29 ka (Kemp et al., 2019). Evidence obtained from the archaeological site of Riwi also indicates that the southern Kimberley became increasingly arid at this time (Whitau et al., 2017; Whitau et al., 2018; Balme et al., 2019). The western Kimberley experienced an active (though variable) monsoon during the LGM, based on the oxygen isotope record from Ball Gown Cave (Denniston et al., 2013) and the faunal and botanical evidence at CG1 (Maloney et al., 2018).

3.2. Stratigraphy and archaeology

Excavation of Widgingarri 1 took place in 1985, with five 1 × 1 m squares dug to a maximum of 112 cm depth in arbitrary spits (Fig. 4) (O'Connor, 1999). Five distinctive layers (numbered 1 to 5 from top to bottom) were identified based on soil compactness, colour change, and organic and shell content. While the lower spits contained a larger quantity of roof spall, bedrock was not reached during the excavation. Fine sandy sediment occurs throughout the deposit, with Layers 5 and 4 containing low amounts of organic material. Sediments are compacted in the lower layers, transitioning to a looser composition 30–40 cm below the surface, with

Table 1
New and previously published radiocarbon ages for Square AA. Ages have been calibrated using OxCal v.4.4 (Ramsey, 2009) and the SHCal20 (Hogg et al., 2020) atmospheric curve for charcoal, and Marine20 for marine shell (Heaton et al., 2020). Calibrated age ranges are given at the 95.4% confidence interval. $F^{14}C$, fraction modern ^{14}C.

Lab code	Sample ID	Sample material	Layer/spit	$F^{14}C$	Radiocarbon age (yr BP)	Calibrated age range (cal. yr BP)	Reference
S-ANU-63825	W1-AA-2	scattered charcoal	2/2	0.9587 ± 0.0024	339 ± 25	449–301	This study
S-ANU-63826	W1-AA-5	scattered charcoal	3/5	0.9789 ± 0.0020	171 ± 22	277– …	This study
S-ANU-63827	W1-AA-9	scattered charcoal	4/9	0.9626 ± 0.0021	307 ± 22	442–285	This study
Wk-1490	W1-AA-7	marine shell	4/7	–	1700 ± 90	1395–954	O'Connor (1999)
S-ANU-63829	W1-AA-13	scattered charcoal	4/13	0.9849 ± 0.0019	122 ± 20	252– …	This study
ANU-5761		$CaCO_3$ encrusted bone	5/18	–	11,910 ± 500	15,469–12,843	O'Connor (1999)
ANU-5762		$CaCO_3$ encrusted bone	5/19	–	9080 ± 600	12,425–8650	O'Connor (1999)
S-ANU-62911	W1-AA-15	bird eggshell	–/15	0.0278 ± 0.00055	28,767 ± 165	33,692–32,256	This study
ANU/AMS 5-10	W1-AA-15	marine shell (*Pinctada* sp.)	–/15	–	18,900 ± 1800	27,287–18,251	O'Connor (1999)
S-ANU-62912	W1-AA-17	marine shell (*Melo* sp.)	–/17	0.0328 ± 0.00056	27,448 ± 144	31,061–30,419	This study
R-11720	W1-AA-17	charcoal/humic acids	–/17	–	modern	–	O'Connor (1999)
R-11795	W1-AA-17	marine shell (*Melo* sp.)	–/17	–	28,060 ± 600	33,006–30,219	O'Connor (1999)

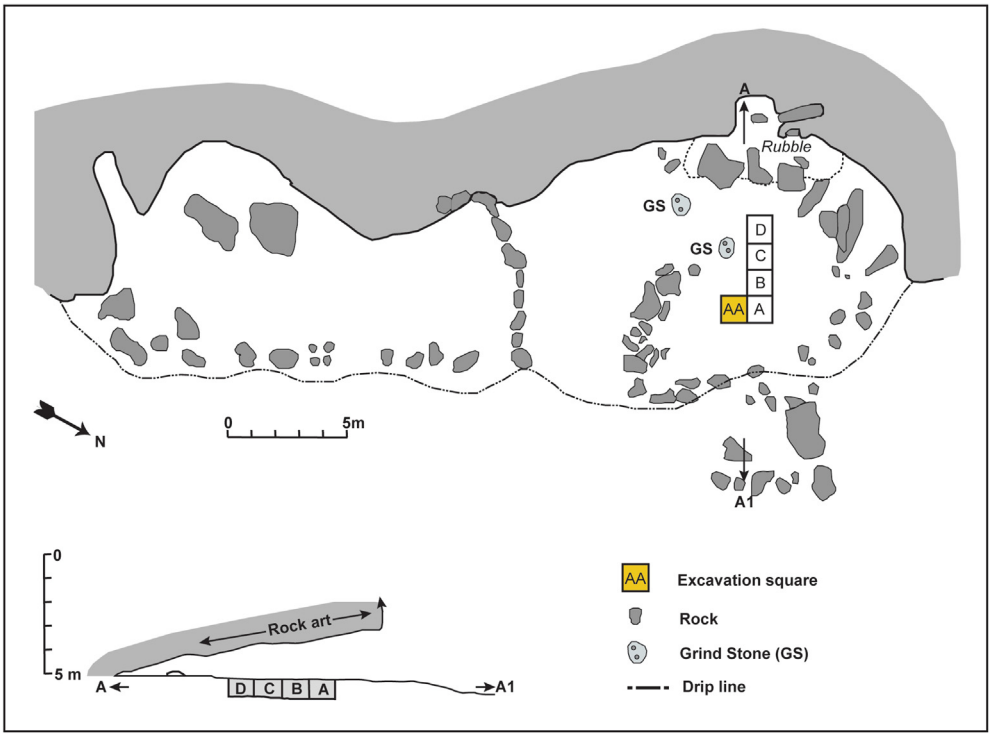

Fig. 3. Site map of Widgingarri 1, showing the location of Square AA, from which the stone artefact assemblage and optical and radiocarbon dating samples originate.

a substantial increase in organic content upwards from this depth.

The lowest recorded layer (Layer 5, spits 19 to 15/14) is lighter in colour than the overlying sediments, being predominantly yellowish-red. The basal spits of Layer 5 in Square AA contain a matrix of calcium carbonate, which is most abundant in the southeast part of the square, cementing the sediments and cultural material. Visible in the southeast section published in O'Connor (1999), and shown in the southeast and southwest sections in R.G.R.'s 1993 field notebook, is a reddish-grey feature (shown as 'F' in Fig. 4) containing calcrete nodules. Found only in Square AA of the site, this feature was excavated as part of Layer 5, with spits 18 to 14/13 cross-cutting both the feature and Layer 5 (Fig. 4). As such, cultural material analysed for these spits may derive from either the feature or Layer 5. Layer 4 (spits 14/13 to 6) overlies Layer 5 and the feature: it is comprised of dark reddish-brown sediments at the bottom, transitioning to dark brown at the top. Layer 3 (spits 5 and 4) is dark brown and records the highest marine shell content of any layer at the site. Layer 2 (spits 3 and 2, dark reddish-grey) and Layer 1 (spit 1, dark brown) have lower shell content and the highest quantities of charcoal and organics.

Detailed descriptions of all finds are reported in O'Connor (1999) and only the broad patterns are summarised here. Charcoal, unburnt plant remains, and fish and mollusc remains are almost non-existent in Layers 5 and 4, but are found in high quantities in Layers 3, 2 and 1. Bone (marsupial and reptile) is preserved throughout the sequence. The artefact assemblage includes unretouched and retouched flakes and flake fragments, including flakes from edge-ground axes (present in Layer 5), with a clear introduction of points (bifacial, unifacial and laterally retouched) in Layer 3. Ground stone axes and basal grinding stones were also found on the shelter floor surface. Unusual finds include jawbone fragments from the now-extinct thylacine (in Layer 4 and in a spit cross-cutting Layer 5 and the feature) and a modified dingo tooth (in Layer 2). A ground sea urchin spine and exotic marine

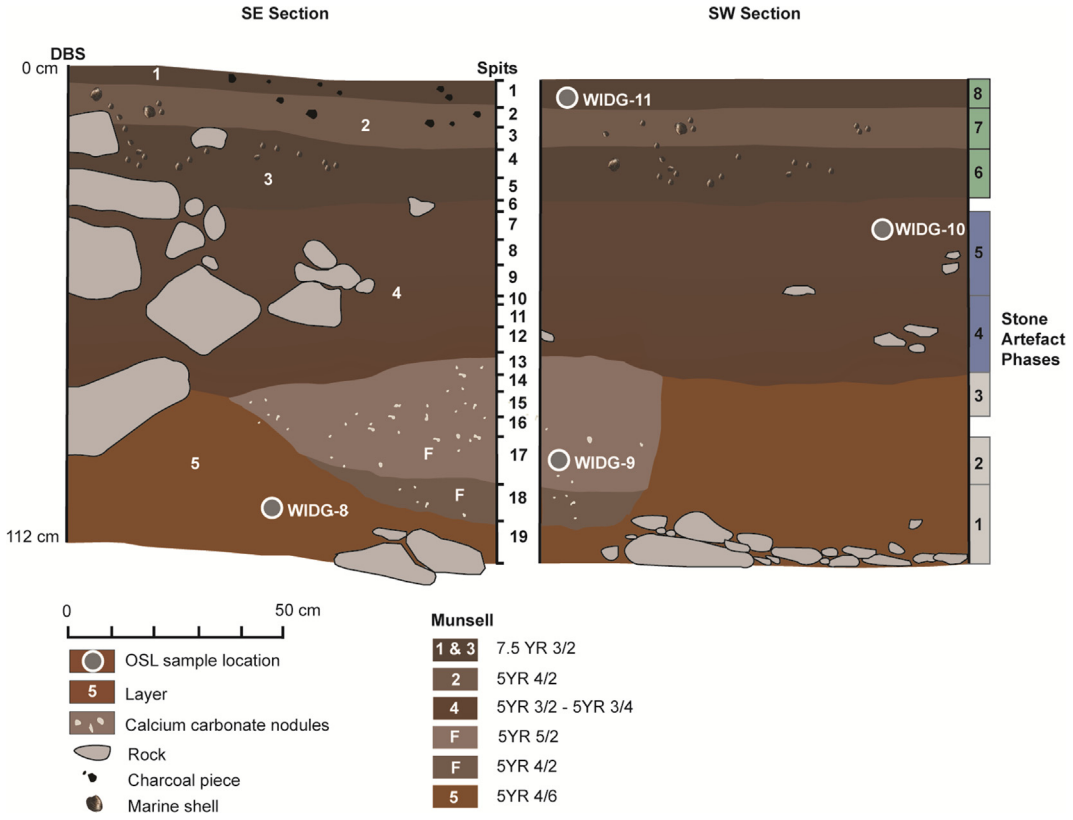

Fig. 4. Stratigraphic profiles of the southeast and southwest walls of Square AA, with locations of optical dating samples indicated, and stone artefact phase boundaries marked. Sections show locations of major layers, from O'Connor (1999) and R.G.R.'s 1993 field notebook.

shells were excavated from the spits cross-cutting Layer 5 and the feature, with bone artefacts found in Layers 3, 2 and 1.

4. Methods

4.1. Radiocarbon dating

For this study, four charcoal fragments, a bird eggshell fragment and a marine baler shell specimen (*Melo* sp.) from Widgingarri 1 Square AA were dated at the Australian National University Radiocarbon Laboratory (lab code S-ANU). The charcoal fragments (not identified to taxa) do not derive from intact hearth features, but were recovered from sieved material and selected for dating on the basis of size and preservation. The marine shell age is on a sample of the same piece dated previously (O'Connor, 1999). Charcoal samples were physically cleaned and crushed to ~1 mm in size, and pretreated with a series of acid (1M HCl, 70 °C, 30 min), base (1M NaOH, 70 °C, 1 h, changing the solution until the base remained colourless) and acid (1M HCl, 70 °C, 30 min) washes. Between each treatment, the charcoal was washed in ultrapure water three times, or until the solution remained colourless. Samples were combusted in a sealed quartz tube in the presence of CuO wire and Ag foil, and the resulting CO_2 was collected and purified cryogenically before conversion to graphite over a Fe catalyst in the presence of H_2 for analysis in a NEC single-stage accelerator mass spectrometer (Fallon et al., 2010). As expected for charcoal, all samples contained more than 60% carbon.

The surfaces of the eggshell and marine shell samples were removed with a Dremel™ drill, and fragments of the cleaned shell were acid leached (0.5M HCl, 70 °C, to remove ~10 wt% and ~50 wt% respectively). These fragments were then reacted with H_3PO_4 in an evacuated Vacutainer™ and the gas collected and dated as described for charcoal. No quality assurance parameters are available for the calcite eggshell. The baler shell was screened using X-ray diffraction (XRD) using a Malvern Panalytical Empyrean Series 3 and analysed over a range of 20–58° 2θ, with step width of 0.0131303° 2θ and a total dwell time of 200 s/step. Phase identification was carried out with the software DiffracPlus Eva 10 (2004) and ICDD PDF-2 database (2004) and phase quantification was performed using HighScore Plus 4.8 (2018). The shell contained 0.3% calcite, which is just above the detection limit of 0.1% calcite, and the age may be underestimated by up to 750 radiocarbon years.

Ages were calculated using a $\delta^{13}C$ value measured by accelerator mass spectrometry (Stuiver and Polach, 1977). Sample preparation backgrounds were subtracted based on measurements of samples of radiocarbon-free CO_2. The new age for the baler shell sample (S-ANU-62912) is statistically indistinguishable from the previous age estimate for sample R-11795 (chi-squared test: df = 1, test statistic T = 1.1, 5% significance level = 3.8).

4.2. Optical dating

Optical dating of sediments provides a means of determining the time since grains of quartz and feldspar were last exposed to sunlight (Huntley et al., 1985; Jacobs and Roberts, 2007; Roberts et al., 2015). As age estimates for artefacts and other archaeological remains are inferred from the depositional ages of the surrounding sediments, rather than being dated directly, it is vital to consider the nature of association between the dated sediments and the items of archaeological interest. Four optical age estimates were obtained from Widgingarri 1. Samples were collected from three distinct layers (Layers 5, 4 and 1), and from the large feature

visible in the southeast and southwest sections, at depths of between 10 and 98 cm (Fig. 4). A sediment sample was also collected at each location for laboratory measurements of radioactivity and moisture content.

Quartz grains of 180–212 or 90–125 μm in diameter were extracted from the samples using standard procedures (Wintle, 1997). Between 1000 and 1500 individual quartz grains were measured per sample to estimate the equivalent dose (D_e) using the single-aliquot regenerative-dose (SAR) procedure (Galbraith et al., 1999; Murray and Wintle, 2000). The experimental conditions and data-analysis procedures used to measure the optically stimulated luminescence (OSL) signal and estimate the D_e values are given in Supplementary Information, together with information on the equipment (Bøtter-Jensen et al., 2003), grain-rejection criteria (Jacobs and Roberts, 2007) and dose recovery tests (Galbraith et al., 1999) used in this study. The OSL and thermoluminescence (TL) properties of quartz grains from one of the Widgingarri 1 samples (WIDG-8 from Layer 5) have been studied extensively in the development of the SAR procedure (Murray et al., 1997; Wintle and Murray, 1997, 1998, 1999, 2000; Murray and Roberts, 1998; Murray and Wintle, 1998, 1999).

The total environmental dose rates were calculated from the sum of the beta, gamma and cosmic-ray dose rates. Beta dose rates for three of the samples were estimated using a low-level beta counting system (Bøtter-Jensen and Mejdahl, 1988), while the beta dose rate for WIDG-8 was derived from beta counting and high-resolution gamma spectrometry (HRGS). Gamma dose rates from the uranium and thorium decay chains (^{238}U, ^{235}U, ^{232}Th) and from potassium (^{4}K) were estimated from portable gamma spectrometry measurements or, for WIDG-8, from a combination of portable gamma spectrometry and HRGS. The burial age of the grains (in calendar years) was obtained by dividing the D_e of each sample by its corresponding environmental dose rate.

4.3. Stone artefact analysis

Each stone artefact was measured and bagged individually and assigned an artefact number. Artefacts from two spits were lost when the Australian National University Weston Storage Facility was destroyed in the 2003 Canberra bushfires, hence spits 6 and 16 are omitted from the present analysis.

All stone artefacts were classified by material and technological class (core, flake, flaked piece, retouched flake); broken flakes, flaked pieces, and heat pops (pot lids) were not analysed further. Cores were assigned a type, and their length, width and thickness were measured according to orientation along the axis of the main flaking surface. The length of the largest complete scar was also measured. Axial (box) length, medial width and platform thickness were measured on all complete flakes. The number of dorsal scars was then counted and the platform type, dorsal scar pattern, any platform preparation, and the presence of any apparent use-wear under low magnification was noted. To calculate the Scar Density Index (Clarkson, 2013; Shipton and Clarkson, 2015), surface area was estimated on flakes by multiplying axial length by medial thickness. Retouched pieces were assigned a type, their length, width, and thickness were measured according to the axis of the original flake, where discernible; and where not, by positioning the main portion of retouch distally. The height of the largest retouch scar was measured, as was the length of the flake margin that had been retouched. Retouched pieces that were neither shaped nor burinated, but had multiple retouch scars crossing 25% of their surface by length, were designated 'core-on-flake'. Ochre was weighed for each excavation unit and the number of pieces with ground facets or evidence of flaking was noted.

5. Results

5.1. Radiocarbon dating

All charcoal samples from Layers 4, 3 and 2 in Square AA have calibrated radiocarbon ages of less than 500 years (Table 1). The bird eggshell, and the redated baler shell from the original study, have ages of 33.7–32.3 and 31.1–30.4 cal ka BP, respectively. The age for the baler shell (from spit 17) is consistent with the previous estimate of 33.0–30.2 cal ka BP, and overlaps with the age for the bird eggshell (from spit 15). The preferential selection of well-preserved charcoal pieces from sieved material appears to have resulted in a bias towards young, probably intrusive, charcoal from Layer 1. This supports the earlier observation of young charcoal in spit 17 (R-11720). None of the charcoal samples were collected from intact hearth features.

5.2. Optical dating

5.2.1. OSL signals

A total of 5300 individual grains were measured in this study, of which 25.1% (1329 grains) were accepted for D_e determination after rejecting unsuitable grains. The accepted grains emit OSL signals that decay rapidly and to a low level when stimulated by the green laser (Fig. 5A), and the sensitivity-corrected dose-response curves are well described by a saturating exponential function (Fig. 5B). Single-grain D_e values were estimated by projecting the sensitivity-corrected natural OSL signal for each grain on to its corresponding dose-response curve. Further details and additional examples are given in Supplementary Information.

5.2.2. D_e distributions

D_e values for individual quartz grains were obtained for all four samples. The single-grain D_e distributions are overdispersed by between 52 ± 3% (WIDG-8) and 173 ± 14% (WIDG-11) (Table 2). These overdispersion (OD) values are larger than expected for samples comprised of quartz grains that were uniformly well-bleached and deposited at the same time, and that have subsequently remained undisturbed (see, for example, Table 4 in Arnold and Roberts, 2009). The D_e distributions are shown as radial plots (Galbraith et al., 1999) in Fig. 6. For the two deepest samples, WIDG-8 and WIDG-9, most of the D_e values are tightly clustered and the majority lie within ± 2 standardised estimates of a common value (~48 and 30 Gy, respectively), but there are a few conspicuous outliers with much smaller D_e values; the latter are likely intrusive grains from the younger, overlying deposits. WIDG-10 has a more overdispersed D_e distribution than WIDG-8 and WIDG-9, with multiple discrete D_e components and some outliers, suggestive of post-depositional mixing. The D_e distribution of WIDG-11 has a clearly delineated baseline (note that 67 negative values are not shown in this plot), with most of the D_e values falling between ~0.4 and 2 Gy, but extending up to ~30 Gy. The distribution pattern for WIDG-11 is consistent with a young sample mixed with older grains.

To estimate the sample D_e values, the finite mixture model (FMM; Roberts et al., 2000) was applied to the single-grain D_e distributions of WIDG-8, WIDG-9 and WIDG-10 to determine the number of discrete D_e components, the relative proportion of grains in each component, and the weighted mean D_e value and associated standard error of each component. The minimum number of statistically supported D_e components was estimated

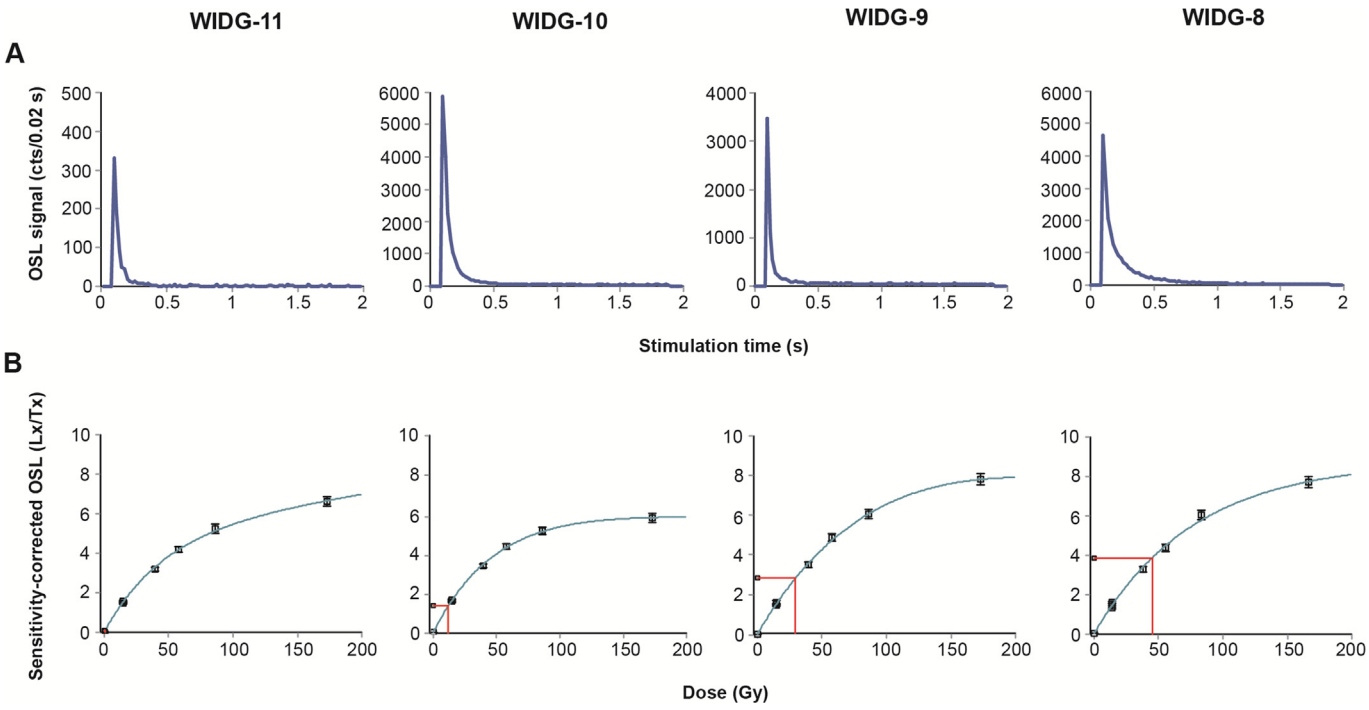

Fig. 5. **A**, OSL decay curves of the natural signal measured for a representative grain from each of the four samples. **B**, Corresponding sensitivity-corrected dose-response curves for each grain, with the sensitivity-corrected natural OSL signals projected on to the curves to show the corresponding D_e estimates.

Table 2
Dose rate data, equivalent dose (D_e) and overdispersion (OD) values, and optical ages for quartz samples from Square AA.

Sample code	Layer/spit	Grain size (μm)	Environmental dose rate (Gy/ka)				Number of grains[b]	D_e (Gy)[c]	OD (%)[d]	Statistical model[e]	Optical age (ka)[f]
			Beta	Gamma	Cosmic	Total[a]					
WIDG-11	1/1	212–180	0.38 ± 0.02	0.29 ± 0.02	0.08 ± 0.01	0.78 ± 0.03	1400/542	0.37 ± 0.02	173 ± 14	MAMul (66%)	0.48 ± 0.03
WIDG-10	4/7	212–180	0.43 ± 0.02	0.39 ± 0.02	0.08 ± 0.01	0.94 ± 0.03	1000/196	13.1 ± 0.8	73 ± 4	FMM (61%)	13.9 ± 1.0
WIDG-9	–/17	212–180	0.41 ± 0.02	0.38 ± 0.02	0.08 ± 0.01	0.90 ± 0.03	1500/206	29.8 ± 0.9	56 ± 3	FMM (94%)	33.0 ± 1.7
WIDG-8	5/18	125–90	0.47 ± 0.02	0.39 ± 0.02	0.08 ± 0.01	0.97 ± 0.03	1400/385	48.2 ± 1.4	52 ± 3	FMM (95%)	49.5 ± 2.3

[a] Sum of beta and gamma dose rates from the surrounding sediment, the contribution from cosmic rays, and an internal dose rate of 0.03 ± 0.01 Gy/ka for each sample. The 1σ uncertainty is the quadratic sum of the random and systematic errors.
[b] Number of grains measured/accepted for D_e determinations after application of the grain-rejection criteria.
[c] Modelled D_e ± 1σ uncertainty.
[d] Overdispersion (OD) refers to the spread in D_e values remaining after accounting for measurement uncertainties.
[e] Statistical models used to estimate the sample D_e values (MAMul, unlogged minimum age model; FMM, finite mixture model). Values in parentheses indicate the proportion of fully bleached grains (MAMul) or proportion of grains in the main D_e component (FMM).
[f] Mean age ± 1σ uncertainty, calculated as the quadratic sum of all known and estimated sources of random and systematic error.

using maximum log likelihood and the Bayes Information Criterion (BIC), which yielded OD values of 30% (WIDG-8), 36% (WIDG-9) and 28% (WIDG-10) for the optimum fits (Galbraith and Roberts, 2012). The dominant D_e component in each of these samples (i.e., the component containing the largest proportion of grains: 95% in WIDG-8, 94% in WIDG-9 and 61% in WIDG-10) was used for final D_e and age determination. The WIDG-8 and WIDG-9 distributions both contain a secondary component (5–6% of grains) with much smaller D_e values, whereas the remaining ~40% of D_e values in the WIDG-10 distribution are split between higher and lower D_e components. The latter (~5 Gy) is consistent with the secondary D_e components in WIDG-8 and WIDG-9, and the higher D_e component (~40 Gy) is similar in size to the main D_e component in WIDG-9.

The unlogged minimum age model (MAMul; Arnold et al., 2009) was used to determine the weighted mean D_e value for the low-dose population of grains (assumed to be the most fully bleached) in the truncated D_e distribution of WIDG-11. This model enables measured values that are zero or negative (i.e., values with errors consistent with a D_e of 0 Gy) to be incorporated in the final D_e estimate. Before running the model, an OD value of 30% was added in quadrature to the D_e measurement error for each grain, based on the optimal OD estimates obtained by the FMM for the other three samples. The MAMul estimates the proportion of fully bleached grains in the WIDG-11 distribution as ~66%, which includes positive and negative D_e values consistent with 0 Gy at 2σ (~44% of the total number); such grains are indistinguishable from modern.

5.2.3. Environmental dose rates

The dose rates for all four samples are presented in Table 2. Measured water contents were on average ~3%, but we used 5% as the average long-term water contents for final dose rate and age determinations (see Supplementary Information). WIDG-8 was measured using HRGS to assess whether the ^{238}U and ^{232}Th day series are in secular equilibrium, and to measure the ^{4}K activity. In the ^{238}U chain, the activities of ^{238}U, ^{226}Ra and ^{210}Pb were estimated

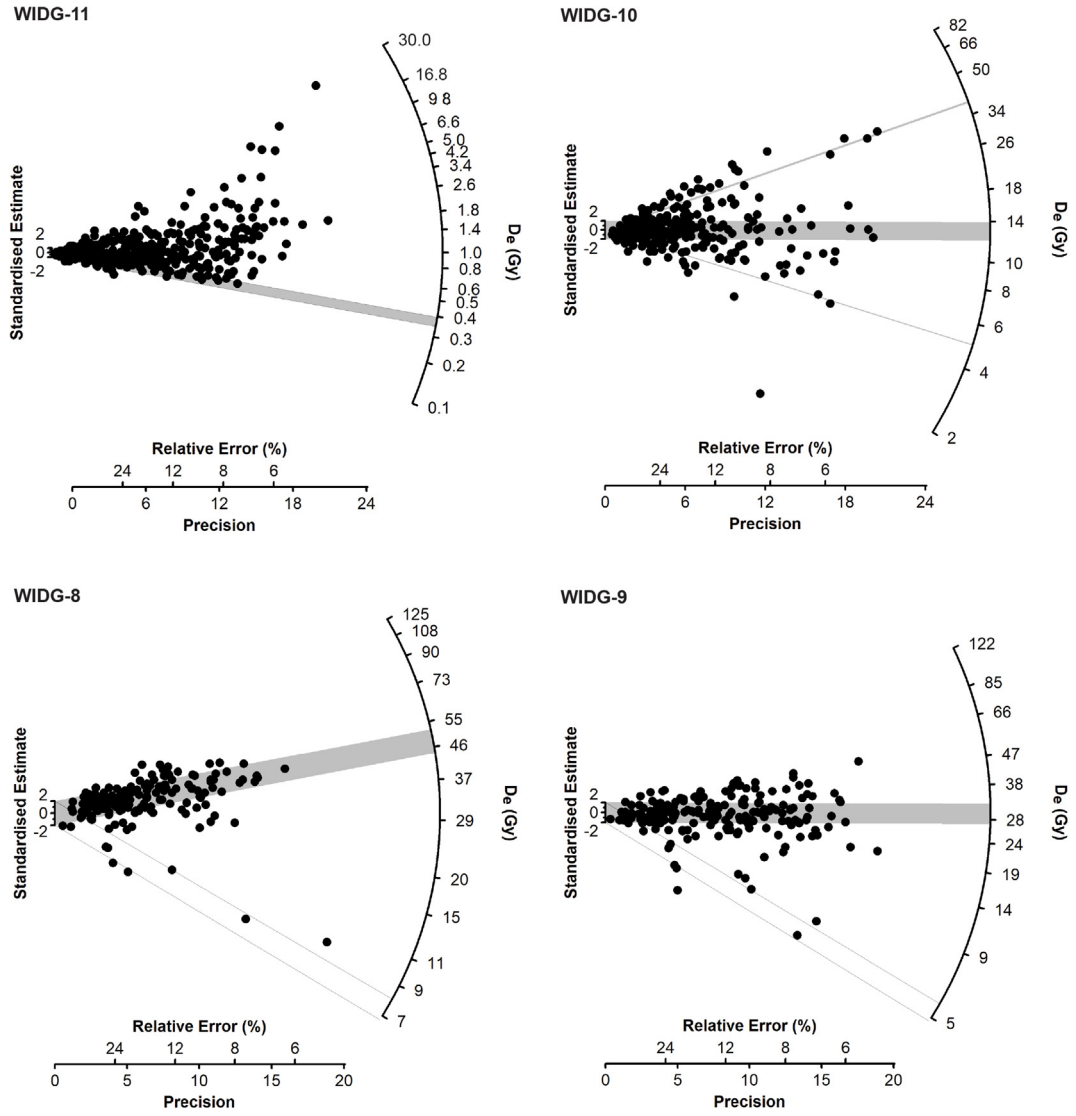

Fig. 6. Distributions of D_e values for single grains of quartz from sediment samples collected from Square AA. Radial plots are shown in order of increasing depth (clockwise from top left). For WIDG-10, WIDG-9 and WIDG-8, the grey band is centred on the main D_e component (as determined by the FMM and used for age estimation), and the minor D_e components are denoted by single lines (WIDG-10) or unfilled bands (WIDG-9 and WIDG-8). For WIDG-11, the grey band is centred on the D_e estimate obtained using the MAMul. Negative values are not shown in this plot, because the radial axis has a logarithmic scale, but they are included in the MAMul D_e estimate.

as 20.54 ± 2.07, 20.88 ± 0.38 and 16.34 ± 2.44 Bq/kg, respectively, while those of ^{228}Ra and ^{228}Th in the ^{232}Th chain were estimated as 18.23 ± 0.75 and 17.97 ± 0.37 Bq/kg; the measured ^{4}K activity was 78.81 ± 4.22 Bq/kg. There is no evidence of present-day disequilibrium in the ^{232}Th chain or between ^{238}U and ^{226}Ra in the ^{238}U chain, but the ^{210}Pb/^{226}Ra ratio of 0.78 ± 0.12 indicates that there may be disequilibrium of ~20% (significant at 1σ but not 2σ). Any disequilibrium present between ^{226}Ra and ^{210}Pb is likely due to the loss of radon gas (derived from the decay of ^{226}Ra), which is common in sedimentary deposits (Olley et al., 1996; Olley et al., 1997). The gamma-ray dose rates measured using HRGS and in situ gamma spectrometry (both adjusted to a water content of 5%) are statistically indistinguishable (0.99 ± 0.07), as are the beta dose rates estimated from HRGS and beta counting (1.06 ± 0.09). For WIDG-8, therefore, we combined each pair of independent estimates of beta and gamma dose rate to determine the final values, and we used in situ gamma spectrometry and beta counting for the other three samples. Use of emission-counting methods implicitly assumes that the present state of (dis)equilibrium in the U and Th chains has prevailed throughout the period of sample burial, but most time-dependent disequilibria are unlikely to give rise to errors in the total dose rate of more than a few percent (e.g., Olley et al., 1996; Olley et al., 1997). Field measurement of the gamma dose rate also allows for any spatial inhomogeneity within ~30 cm of each sample.

5.2.4. Optical ages

The optical ages of the Widgingarri 1 sediments are in stratigraphic order, increasing with depth from 0.48 ± 0.03 ka (Layer 1) to 49.5 ± 2.3 ka (Layer 5) (Table 2). Sample WIDG-8 from the lowest layer (Layer 5) appears to have remained largely intact since deposition, with only a few younger intrusive grains present in its D_e distribution (Fig. 6). The age for the reddish-grey feature from which WIDG-9 was collected is mostly comprised of grains with similar D_e values that yield a significantly younger age (33.0 ± 1.7 ka), with little evidence for mixing between the infill feature and the underlying deposit. The age for the feature is consistent with the two radiocarbon ages from this depth (Table 1), which suggests

that the eggshell and baler shell samples may have derived from the feature. Their provenance remains uncertain, however, due to the cross-cutting of Layer 5 and the infill feature. There appears to be a significant hiatus in sediment deposition between Layers 5 and 4, with the upper part of Layer 4 dated to 13.9 ± 1.0 ka (WIDG-10). The two minor D_e components in WIDG-10 yield ages consistent with those of the underlying infill feature and the sediments overlying Layer 4, suggesting the incorporation of older and younger grains in this sample via post-depositional mixing. This is supported by young charcoal from Layers 2–4, and the presence of an intrusive piece of modern glass in the upper part of Layer 4. No sediment samples for optical dating were obtained from the shell midden in Layer 3, or from the overlying Layer 2. Midden building along the Kimberley coastline to the south of Widgingarri 1 began at ~5 ka (Figs. 1B and 2D), so the Widgingarri 1 midden likely dates to around this time (consistent with the optical age of 5.2 ± 0.6 ka for the low-D_e component in the WIDG-10 distribution) or later. WIDG-11 from Layer 1 shows evidence of extensive mixing (Fig. 6), with the youngest population of well-bleached grains deposited ~500 years ago. This layer is likely to be the source of the charcoal samples dated to ~500 years and younger (Table 1).

5.3. Artefact assemblage

The stone artefact assemblage from Square AA was divided into eight phases based on material and technology (Fig. 4). Table 3 provides information on the corresponding layers and spits for each phase, as well as the proportions of key technological and typological components. Material changes are depicted in Fig. 7 and the dominant and distinctive materials and technologies are summarised for each technological phase in Table 4. In total, 2535 excavated stone artefacts were recorded, comprised of 1501 flakes, 774 broken flakes, 126 flaked pieces, 53 cores, 41 retouched flakes, 30 grinding stones and mullers, 8 chert pot lids, and 2 quartz manuports. The lowest spit (spit 19) contained 56 artefacts. Knapped stone artefacts were made from six materials (Fig. 7, Table 4). The most frequent were a pale quartzite ranging from white to yellow in colour and a fine dark ferruginous quartzite, which were probably both available in the suite of Proterozoic local quartz sandstones that vary in granularity and colour within a few kilometres of the site (Green et al., 2017). Chert was also frequently used and may have been available in the same sedimentary formations as the quartzite, but chert typically occurs in smaller and scarcer packages. There was a moderate frequency of quartz and volcanic artefacts; the latter are likely basalt, which is not locally available, the nearest volcanic geology occurring ~15 km inland (east) of the site. Four chalcedony artefacts are present in phase 5; given there is only one other occurrence of this very fine-grained material (in phase 6), we presume it is exotic. Glass is present in spits 1–3 (phase 8), with a single specimen in spit 8 likely intrusive.

Cores throughout the sequence are relatively informal single-platform, multi-platform and bipolar pieces with occasional discoidal cores and core-on-flakes. Likewise, platform types display a similar range throughout the sequence, with >3% of each of single, multiple, focalised and crushed platforms in every phase. Overhang removal was used to prepare >3% of platforms in every phase. Retouch is typically informal, with scrapers, notches and ventrally retouched pieces common, but formal types (e.g., unifacial points) first appear in the assemblage in phases 6–8 (Table 3). The principal diachronic trends in knapping technology appear to be related to these shaped artefacts and the relative emphasis on axes, as well as changing provisioning strategies. Platform faceting becomes common in phases 7 and 8 (Table 3).

Fragments of mullers and grinding stones occur in phases 2–5 and 7 (Table 3), with two intact grinding stones located on the surface of the site (Fig. 2). The five muller fragments all have rounded grinding surfaces. The ground surfaces of the grindstones are typically flat with a mean thickness of 9.88 mm, though this is an underestimate as most do not preserve the opposing surface. The most complete grindstone is small, with a maximum length of 64.22 mm. One fragment from phase 2 is coated in red ochre residue (Fig. 8F). Ochre occurs in phases 2–8, with very low quantities in phase 6. A total of 222.9 g of ochre was recovered, including 10 ground pieces with macroscopic striations and 5 flaked pieces (Fig. 8E). The ochre is predominantly haematite, with smaller quantities of red shale and mica.

Ground stone axe technology is represented by volcanic flakes with ground facets on their dorsal surfaces, with the highest proportions occurring in the early part of the sequence in phases 1–2, and very few found in the middle of the sequence (phases 3–6) (Table 3, Fig. 7). Of the 134 complete volcanic flakes, 36 (27%) have ground facets on their dorsal surface or platforms (Fig. 8A–D). Complex dorsal scar patterns, with removals from the opposite direction to the flake itself or from three or more different directions, account for 29% of the complete volcanic flakes (where scar pattern was discernible, $n = 90$). Unlike the other four main raw materials, no volcanic flakes were retouched. Volcanic flakes with unground dorsal surfaces were far more likely than the general flake population to be tertiary flakes without any cortex (93% versus 65%, $\chi = 35.171$, $p < 0.001$, $n = 1475$), indicating working of volcanic stone was focussed particularly on later stages of reduction. Dorsal scar patterning, together with a lipped initiation on a volcanic flake with a ground platform, aligns with volcanic flakes being struck from bifacially shaped axe blanks.

A transition in material selection occurs in the middle of the Widgingarri 1 lithic sequence, with increased use of cryptocrystalline chert in phase 3, increased use of ferruginous quartzite in phase 4, and increased use of cryptocrystalline quartz in phase 5. Chi-squared tests showed significant decreases in the proportion of microcrystalline pale quartzite relative to other materials (excluding volcanic) between phase 2 (50%, $n = 323$) and phase 3 (29%, $n = 120$) ($\chi = 16.055$, $p = 0.000062$, $n = 443$), and again

Table 3
Numbers and proportions of key artefact types and technological features by phase.

Layer	Spit	Phase	Axe flakes	Platform faceting	Lipped initiations	Bipolar cores	Points	Grinding stones	Ground ochre
1	1	8	1 (3%)	14 (59%)	26 (93%)	1 (3%)	1 (12.5%)	0	1 (10%)
2	2–3	7	7 (18%)	5 (21%)	0	1 (3%)	4 (50%)	2 (7%)	0
3	4–5	6	1 (3%)	1 (4%)	0	1 (3%)	2 (25%)	0	0
4, Upper	7–9	5	2 (5%)	0	0	22 (69%)	1 (12.5%)	9 (30%)	2 (20%)
4, Lower	10–13	4	3 (8%)	1 (4%)	0	5 (16%)	0	12 (40%)	2 (20%)
5, Upper	14–15	3	3 (8%)	0	0	2 (6%)	0	1 (3%)	2 (20%)
5, Mid	17	2	14 (37%)	1 (4%)	0	0	0	6 (20%)	3 (30%)
5, Lower	18–19	1	7 (18%)	2 (8%)	2 (7%)	0	0	0	0
Totals			**38 (100%)**	**24 (100%)**	**28 (100%)**	**32 (100%)**	**8 (100%)**	**30 (100%)**	**10 (100%)**

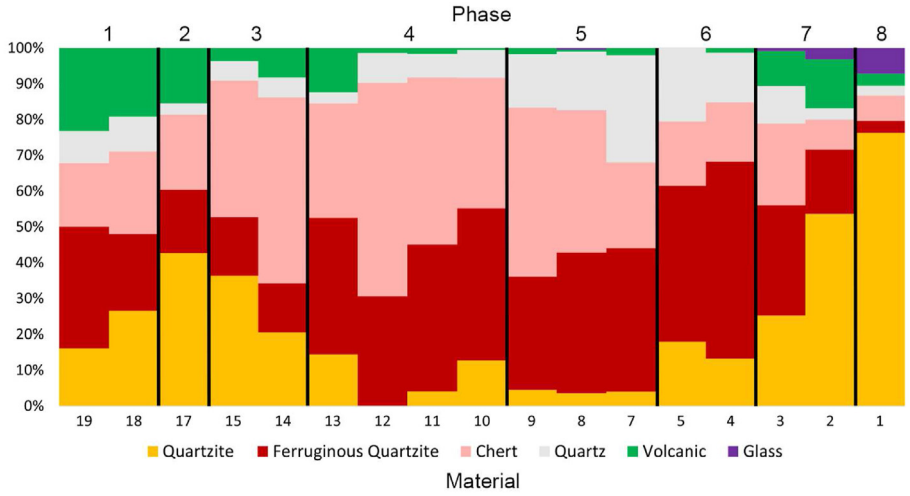

Fig. 7. Proportions of lithic materials by spit (numbered along the bottom) and phase (numbered along the top) for Square AA.

Table 4
Phasing of lithics from Square AA with raw materials, types and attributes.

Phase	Number of lithics	Dominant and distinctive materials	Distinctive types and attributes
8	295	Pale quartzite, glass	Ground platforms, lipping
7	218	Pale quartzite, glass	Points, faceting, grinding stones
6	190	Ferruginous quartzite, quartz	Points, tula
5	534	Chert, quartz	Grinding stones
4	473	Chert, ferruginous quartzite	Grinding stones
3	130	Chert, pale quartzite, basalt	Grinding stones
2	383	Pale quartzite, basalt	Grinding stones
1	312	Ferruginous quartzite, basalt	

between phases 3 and 4 (9%, n = 456) (χ = 32.669, p < 0.00001, n = 576). Cores are more common in the middle part of the sequence, with chi-squared tests showing significant increases in the proportion of cores between phases 2–3 (1%, n = 503) and phase 4 (3%, n = 473) (χ = 4.145, p = 0.042, n = 976), and again between phases 4 and 5 (5%, n = 554) (χ = 4.021, p = 0.045, n = 1027). Only 6% (n = 53) of cores from the entire assemblage were made on the pale quartzite, compared with 22% (n = 1542) of flakes and flaked pieces. Mean core length for the whole Widgingarri 1 Square AA assemblage was just 17.34 ± 11.47 mm, with the majority of cores (76%) from phase 5 being bipolar. A Mann-Whitney *U* test indicated that the last flake scar travelled across a greater proportion of the cores' length on bipolar versus non-bipolar cores (U = 187, p = 0.041, n = 50), such that bipolar flaking appears to have been used to maximise flake size on small cores.

Shaped tools, including a tula adze slug and several point types, appear in phases 6–8 (Fig. 9). In phase 6, the three shaped tools consist of a tula slug (Fig. 9C) and the broken proximal sections of a bifacial and a unifacial point. In phase 7, there are three unifacial points (one complete, two broken) and three bifacial points (two complete, one broken). Phase 8 contains the broken butt of a Kimberley point (Fig. 9D). The appearance of shaped tools occurs alongside a progressive growth in the use of pale quartzite (Fig. 7), with chi-squared tests showing significant increases in this material between phases 5 and 6 (χ = 21.953, p < 0.00001, n = 724), and between phases 6 and 7 (χ = 29.87, p < 0.00001, n = 408). This is matched by a significant decrease in the proportion of cores between phase 5 and phases 6–8 (χ = 25.763, p < 0.00001, n = 1226). Between phases 1–5 and phases 6–8 there is a significant reduction in flake area (unequal variances *t*-test for area, F = 58.777, t = −11.734, df = 1523.2, p < 0.001, mean difference = 111 mm^2) and an increase in scar density (unequal variances *t*-test, F = 67.61, t = 11.046, p < 0.001, mean difference = 10.6 scars per square inch). This is likely because many of the flakes in the later phases were removed by fine retouching of the shaped tools. A bone artefact from phase 6 may be for retouching shaped tools (Fig. 9A).

Other than the volcanic flakes related to axe working, lithics throughout the sequence may be regarded as miniaturised (Pargeter, 2016; Shipton et al., 2021). Imported fine-grained materials dominate, and mean complete flake length is consistently <15 mm (Fig. 10). This miniaturisation persists despite the differences in material selection and knapping technology between the early and middle part of the sequence. Mean flake length (13.64 ± 7.24 mm) for phases 1–5 corresponds to mean final scar length on cores (12.6 ± 5.93 mm) (equal variances *t*-test, F = 2.999, t = 0.967, df = 1141, p = 0.334), suggesting these values approximate optimal minimum flake size, with cores discarded at this size threshold. The emphasis on shaped tools is evident in the reduction in flake length in phases 6–8 (Fig. 10) (unequal variances *t*-test, F = 74.106, t = 14.401, df = 1182.5, p < 0.001, mean difference = 4.46 mm), with many of the very small flakes from this upper part of the sequence resulting from retouch.

6. Discussion

6.1. Widgingarri 1 chronology

The four optical ages reported here for Widgingarri 1 provide snapshots of the timing of sediment deposition, but the coarse resolution of the sampling—four samples over a depth of ~112 cm of deposit—prevents meaningful insights into the rates of

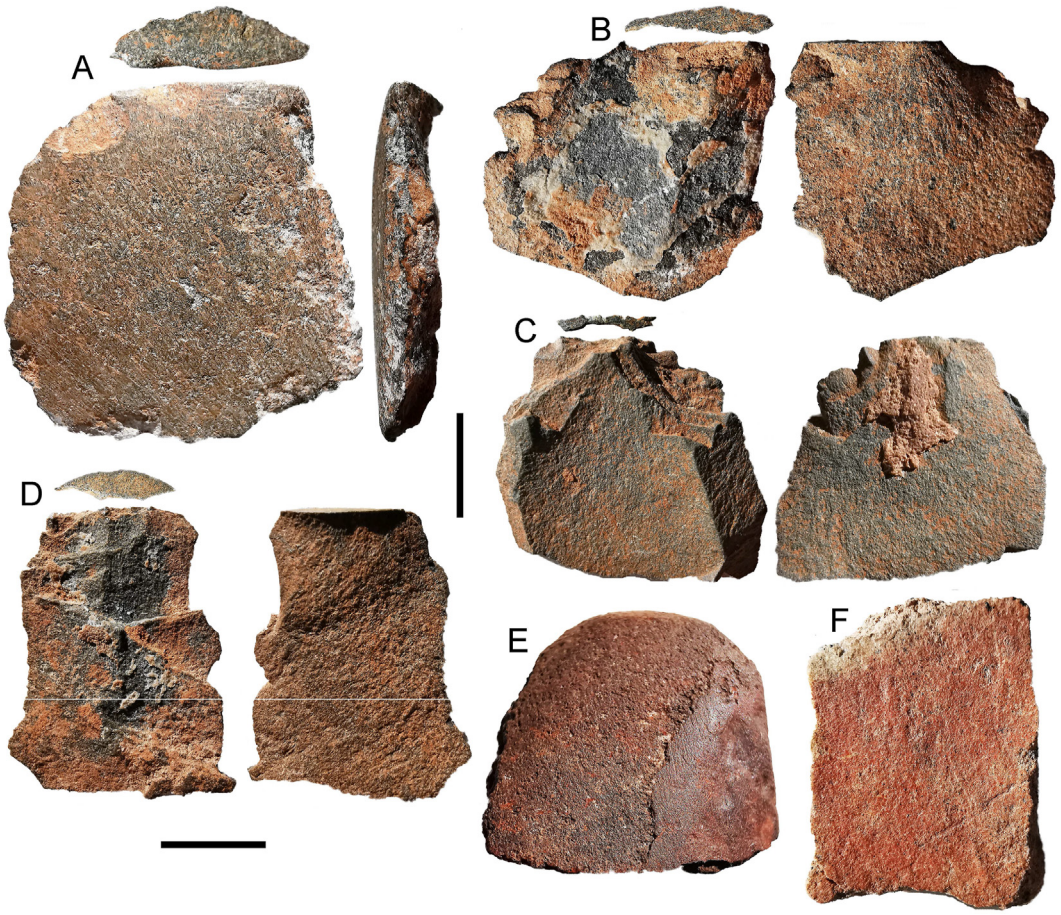

Fig. 8. Artefacts from Square AA. Scale bars are 1 cm. **A**–**D**, Volcanic axe flakes from phase 1 with ground platforms. **A** and **D** have ground dorsal surfaces and lipped initations. **E**, Ground haematite from phase 3. **F**, Grinding stone fragment from phase 2 with ochre coating the ground surface.

sedimentation at the site and the durations of time gaps. In addition, the infill feature in Square AA, dated to ~33 ka, was not observed in any of the other four excavation squares, so the current chronology does not account for spatial variations within the site. The infill feature post-dates Layer 5, for which an age of ~50 ka was obtained for the second deepest spit (spit 18), and is overlain unconformably by Layer 4. The top of Layer 4 was deposited ~14 ka, so this layer represents ~30 cm of sediment deposited over a period of ~19,000 years or less. If the Widgingarri 1 shell midden in Layer 3 is representative of the broader regional pattern of midden building, which began in the Kimberley during the mid-Holocene (Fig. 2D), then it is likely to be considerably younger than the top of Layer 4. Layer 2 remains undated, but is likely to be late Holocene in age, while the uppermost layer (Layer 1) formed within the last 500 years.

The nature of site formation at Widgingarri 1 may be similar to that at the southern Kimberley site of Riwi, where different layers represent punctuated episodes of sediment deposition, separated by time gaps. Deposits between ~30 ka and late Holocene in age are largely absent at Riwi, represented only by small isolated lenses and hearth features dated to the LGM and mid-Holocene (Wood et al., 2016). In contrast, extensive LGM deposits exist near the rockshelter entrance inside the dripline, with the discontinuities interpreted to be the result of erosion by water flowing through the site (Balme et al., 2019). At Widgingarri 1, the infill feature and the evidence for water flow across the floor of the rockshelter (O'Connor, 1999) potentially point to similar erosional processes affecting the deposit.

The chronological resolution of the Widgingarri 1 sequence, the presence of the infill feature, and the possibility of substantial post-depositional erosion have implications for the technological phases recorded in the preserved deposits. The artefacts in the earliest phase (phase 1) may be as old as 49.5 ± 2.3 ka, or possibly older given the recovery of more than 50 artefacts from the lowest spit of phase 1 (spit 19), which appears to underlie the infill feature. However, the provenance of artefacts from the upper spit of phase 1 (spit 18) and from phases 2 and 3 cannot be ascertained with certainty, as spits 18 to 14/13 cross-cut both the feature and Layer 5. As such, the patterns observed within phases 1–3 should be treated with caution, pending further excavation.

6.2. Assemblage interpretation

To avoid over-interpretating the lithic sequence, we separate it here into three broad categories: Late Pleistocene (Layer 5), terminal Pleistocene (Layer 4) and Holocene (Layers 3, 2 and 1). While volcanic flakes with ground facets on their dorsal surfaces are present in every occupation phase, indicating long-term continuity in ground stone axe use, evidence for this technology is most abundant in the Late Pleistocene levels of the site. The low proportion of volcanic flakes with cortex, and the high proportion with ground dorsal surfaces or platforms, indicate a focus on the later stages of reduction, and axe resharpening. The numerous axe-related flakes in the early phase of occupation of Widgingarri 1

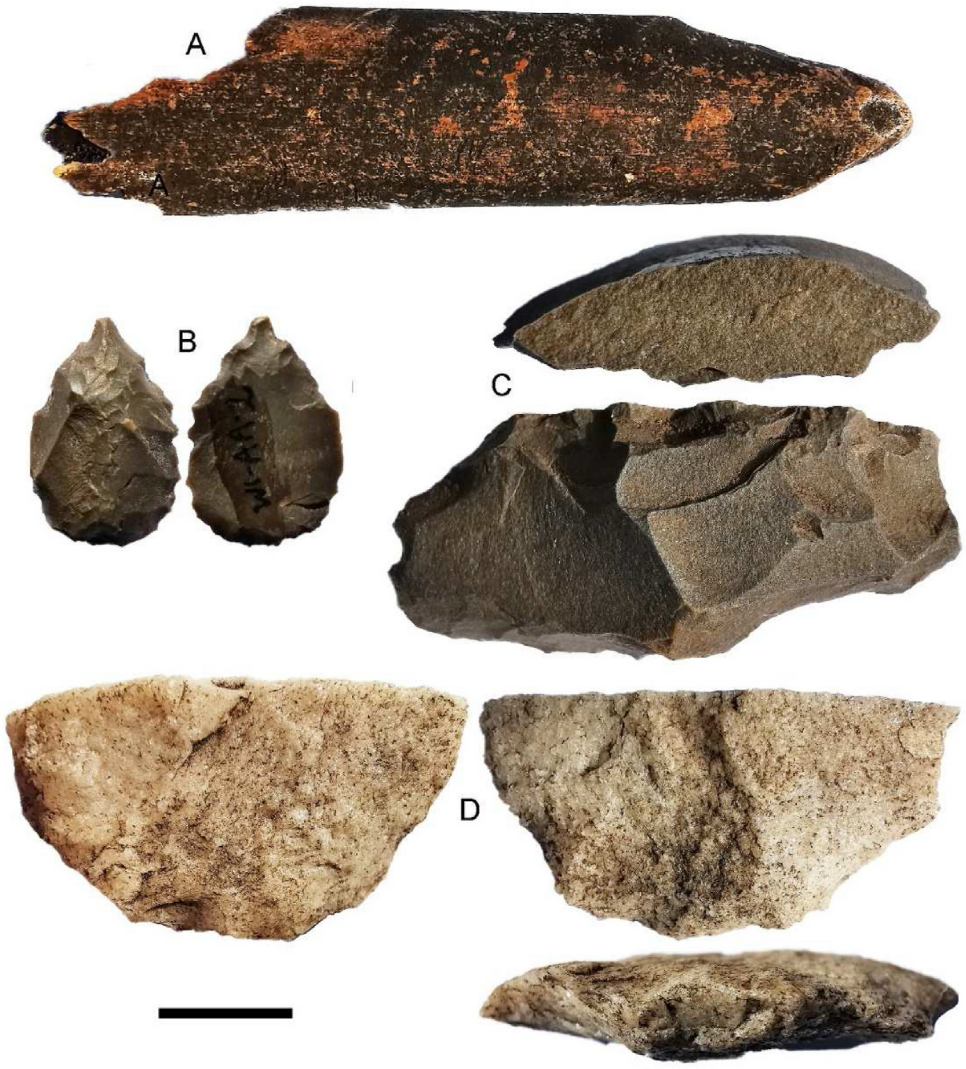

Fig. 9. Artefacts from Square AA, phases 6–8. Scale bar is 1 cm. **A**, Bone retoucher from phase 7. **B**, Chert bifacial point from phase 7. **C**, Ferruginous quartzite tula slug from phase 6. **D**, Broken butt of a pale quartzite Kimberley point from phase 8.

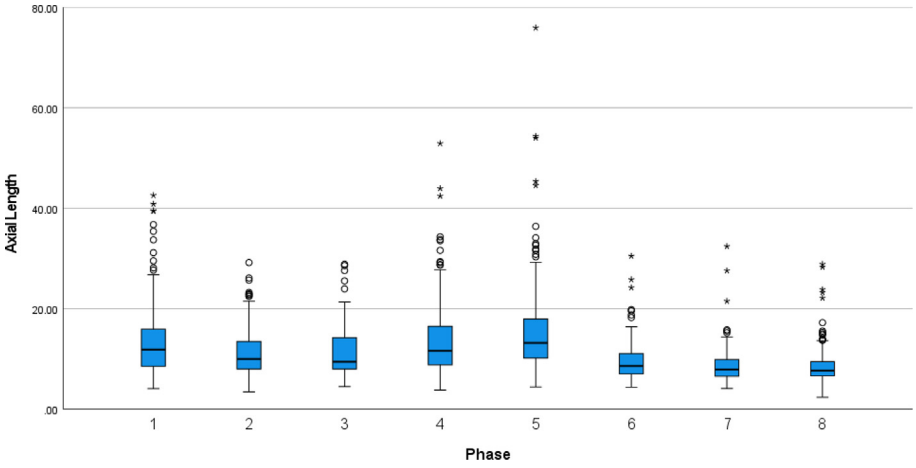

Fig. 10. Boxplot of complete flake length in mm (excluding volcanic flakes) from Square AA.

indicates that, as elsewhere in the Kimberley (Hiscock et al., 2016) and western Arnhem Land (Clarkson et al., 2017), this complex technology was actively used at this time. Another feature of the flaked stone technology throughout the sequence is the creation of miniaturised flakes, something that Widgingarri 1 has in common with sequences covering the same MIS 3–1 time span in Wallacea (Shipton et al., 2019; Shipton et al., 2021).

The terminal Pleistocene (Layer 4) artefact assemblage at Widgingarri 1 shows a notable trend towards increasing mobility, with an increase in the import of the cryptocrystalline materials (chert, quartz and chalcedony) that tend to occur as small and scarce clasts. This transition corresponds with the appearance in the faunal record of the arid-adapted bilby (O'Connor, 1999). An increase in the proportion of cores through the terminal Pleistocene (peaking in the upper part of Layer 4) suggests that much knapping and discard of flakes took place off-site, and that cores were preferentially curated before being discarded at the site when exhausted. Bipolar cores increase through time in Layer 4. This technology is suited to maximising flake production from small transported cores approaching the end of their use life (Hiscock, 1994; Pargeter and Eren, 2017).

The Holocene layers are distinguished by the emergence of several important technology types and the formation of the shell midden. A reduction in the import of cryptocrystalline materials and cores in Layers 3, 2 and 1 is likely due to reduced mobility at the site, as observed elsewhere in the Australian record at this time (Clarkson, 2007). Rising sea levels resulted in the coastline reaching its present position, ~2 km from Widgingarri 1, at ~8 ka (Williams et al., 2018), with the adjacent shelter of Widgingarri 2 yielding evidence for the exploitation of marine shell and other coastal resources from about this time (O'Connor, 1999). Marine shellfish and fish were extensively exploited when Layer 3 was deposited at Widgingarri 1 (O'Connor, 1999), indicating increased proximity to marine environments. Midden building on the modern Kimberley coast began at ~5 ka (Fig. 2D), when the coast at Widgingarri would have been close to or at its present position. Layer 3 likely dates, therefore, to the mid-Holocene.

This interpretation is supported by the first appearance of intensively retouched implements, including points and tula adze technology (as well as the very small flakes from their retouch), at the onset of deposition of Layer 3. Points and tula adzes date to the mid-to-late Holocene in the Kimberley and elsewhere in Australia (Fig. 2E) (Bowdler and O'Connor, 1991; Hiscock, 1994; Clarkson, 2007; Maloney et al., 2017). Layer 2 marks the beginning of Kimberley point production at the site, with Layer 1 containing several technological changes associated with the manufacture of this distinctive technology, perhaps in part as trade items (Akerman et al., 2002; Harrison, 2004). The switch to pressure-flaked Kimberley points in the last 1000 years accords with evidence from elsewhere in the Kimberley (Fig. 2E) (Maloney et al., 2014).

6.3. Fifty thousand years of Kimberley occupation

The new chronology for Widgingarri 1 repositions the site within the Kimberley archaeological sequence. The previously published radiocarbon ages (O'Connor, 1999) placed it within a small group of sites dated to a period between ~32 and 30 ka (Figs. 1 and 2A, yellow). The optical age of 49.5 ± 2.3 ka for Layer 5, however, indicates that initial occupation occurred much earlier, placing it in the first pulse of site establishment across the region (Fig. 1B and 2A, orange). It also expands the geographical range of evidence of human activities in the Kimberley, with early sites now found in the north, south and west. The other three optical ages for the Widgingarri 1 sequence suggest that further and more detailed work at the site may have the potential to shed light on cultural responses to the heightened aridity at the end of MIS 3 and during the LGM, the increase in humidity during the terminal Pleistocene and the Holocene, and the historical period of occupation.

The radiocarbon and optical ages reported here for Widgingarri 1 exemplify the general issue of low chronological resolution of the occupation history of the region. Table S2 provides a full list of age estimates known for sites in the Kimberley region, and all reliable age estimates associated with occupation are displayed in Fig. 11. A few age estimates (shown in grey in Table S2 with explanatory footnotes) are excluded from Fig. 11, either because the TL or optical ages are suspected to have been affected by partial bleaching, or because the radiocarbon ages are thought to have been affected by fluctuating water-table levels or a range of contamination issues. Fig. 11A shows the distribution of ages for the 11 sites that contain evidence for occupation during the Late to terminal Pleistocene, and Fig. 11B shows the distribution of ages for 59 sites with Holocene occupation, further divided into four geographical regions (north, south, east and west).

Most sites—including Widgingarri 1—have too few ages to reconstruct their occupation histories in any detail, or to establish the timing and duration of any stratigraphic breaks. The majority have only 1–3 age estimates, highlighting the problem of dating only selected layers at archaeological sites (e.g., the deepest layers or those containing the largest or best-preserved charcoal fragments). Eight sites in the Kimberley— Borologa 1 in the north, Karlinga 3, Goorurarmum 1, Granilpi and Jinmium in the east, and Mount Behn, Eastern Beach Red Dune (EBRD) Midden and Djura (formerly Windjana Gorge Watertank Shelter) in the west—have records of sufficient resolution to contribute to our understanding of the Holocene occupation history of the region, and three sites—CG1 and CG3 in the west and Riwi in the south—have 'high-resolution' chronologies that allow for robust interpretations of their occupation sequences.

CG1 is the flagship record for the region, with a largely intact sequence spanning most of the last 50,000 years of occupation (Maloney et al., 2018). Riwi has a detailed Pleistocene record, dated using two independent methods (radiocarbon and optical) at sufficient resolution to clearly identify stratigraphic breaks (Wood et al., 2016). The chronological resolution at CG3 is sufficiently high to identify gaps during the LGM and the early to mid-Holocene (O'Connor et al., 2014). In the present study, we have updated the chronological models for CG1 and Riwi (radiocarbon only) using OxCal v.4.4 (Ramsey, 2009), after recalibrating all radiocarbon ages using the SHCal20 (Hogg et al., 2020) and Marine20 (Heaton et al., 2020) curves. The updated chronologies supersede those previously published for these sites. The calibrated ages are presented in Table S2 and the updated Bayesian age models in Figure S2, with the model outputs and OxCal CQL2 codes presented in Tables S6 and S7, respectively. The chronological models for CG1, CG3 and Riwi show the power of detailed dating studies for finer-scale interpretations of the occupation and site-formation histories of sites in the Kimberley region.

6.4. Earliest records of occupation of Sahul

An age for initial occupation of Widgingarri 1 of 49.5 ka, with total uncertainties of 2.3 ka at 1σ and 4.6 ka at 2σ, makes it one of the oldest archaeological sites in Sahul, and brings it into the broader debate on the timing surrounding evidence of first peopling of the continent. Fig. 12 shows the position of Widgingarri 1 in relation to the oldest known archaeological sites from five regions across Sahul (all sites with point estimates of age >46 ka).

In Fig. 12, the boundary probability distribution functions representing the start (blue) and end (orange) Bayesian modelled age estimates for the earliest cultural layer at a site are presented at

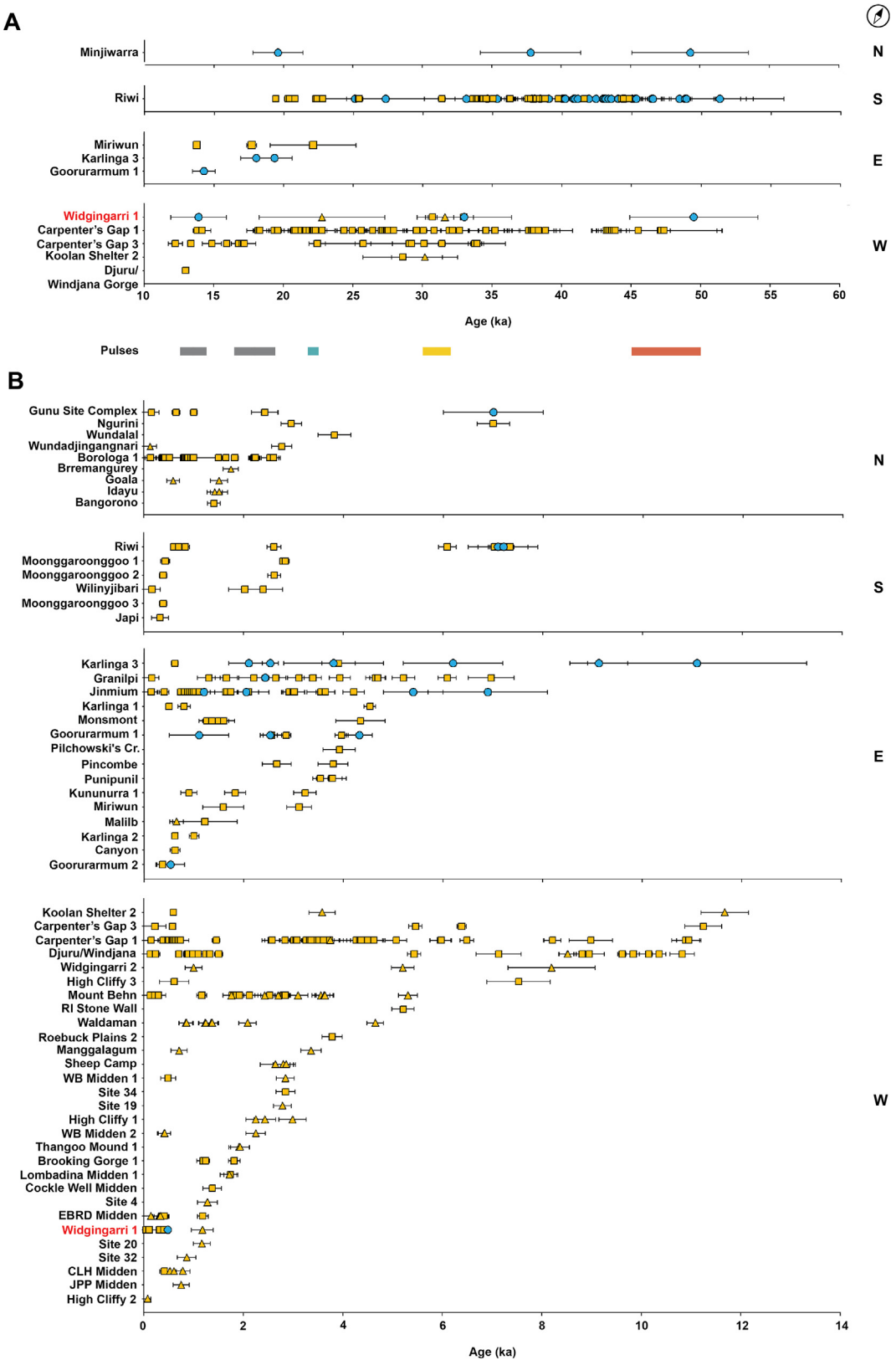

Fig. 11. Age estimates for all known occupation sites in the Kimberley (Table S2). Widgingarri 1 is shown in red. Optical ages are shown as blue circles, radiocarbon ages on charcoal as orange squares, and radiocarbon ages on marine shell as orange triangles. Confidence intervals for all ages are at 95.4% probability. Samples that returned modern ages, and ages associated with culturally sterile sediments, are not shown. **A**, Late Pleistocene to terminal Pleistocene ages. **B**, Holocene ages. RI, WB, EBRD, CLH and JPP refer to Rankin Island, Western Beach, Eastern Beach Red Dune, Cape Leveque Headland and James Price Point, respectively. (For interpretation of the references to colour in this figure legend, the reader is referred to the Web version of this article.)

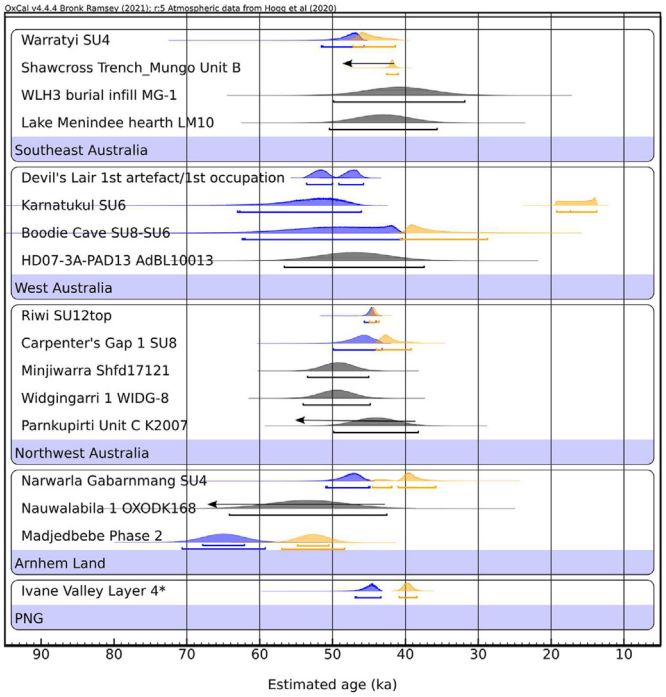

Fig. 12. Probability distributions (95.4% confidence interval) of the Bayesian modelled start (blue) and end (orange) age estimates, and of individual (grey) age estimates, for initial occupation of the oldest known archaeological sites in Sahul. The start and end ages for Devil's Lair correspond to the age estimates for the lowest artefact recovered during excavation and for initial occupation of the cave, respectively. Arrows indicate minimum age estimates. All radiocarbon ages have been calibrated using the latest 2020 calibration curves, and previously published Bayesian age models are updated in this figure. Further details are provided in Supplementary Information, including site-specific age models, model output information and the OxCal CQL2 code used to generate the age models and construct this figure. (For interpretation of the references to colour in this figure legend, the reader is referred to the Web version of this article.)

95.4% probability. The probability distributions shown in grey denote individual age estimates associated with the earliest occupation of sites that have insufficient age estimates to build constrained chronological models (Roberts et al., 1994, this study, Cupper and Duncan, 2006; Olley et al., 2006; Veth et al., 2009; Cropper and Boone, 2018; Veth et al., 2019).

We make four important observations. First, with the sole exception of Riwi, where a charcoal fragment from a combustion feature was dated, age estimates for the earliest occupation of all sites are from materials that are only weakly associated with human activity (e.g., charcoal in sediment) or from quartz grains exposed to sunlight, where association with human activity is inferred. For sites with Bayesian age models, the probability distributions in Fig. 12, therefore, represent the earliest and latest possible age estimates for the human activity that occurred within the dated context. In most cases, it is not possible to ascertain whether occupation occurred continuously throughout the entire unit, or whether it was clustered towards one end of the age range or closer to the middle. The Shawcross Trench at Mungo represents an extreme case: it is not possible to stratigraphically align the dated samples and the artefacts within the same unit, so only the upper boundary age (i.e., a minimum age estimate) for the unit is presented.

Second, the start dates of occupation at Nawarla Gabarnmang and Widgingarri 1 are not associated with the lowermost artefacts recovered from these sites. At Nawarla Gabarnmang, the middle to lower parts of SU4 remains undated, owing to a paucity of charcoal in the deposit (David et al., 2019).

Third, all the radiocarbon ages are close to the effective limit of the technique and susceptible to the effects of small-scale contamination by modern carbon. Some of the charcoal samples dated by radiocarbon were pretreated only with an acid-base-acid protocol (e.g., Ivane Valley), and others include shell or eggshell that has not been, or cannot be, screened for alteration (e.g., Boodie Cave, Warratyi). Although age estimates are consistent and, therefore, likely to be accurate, it is possible that they may underestimate the true age of the deposit. The likelihood of contamination has been explicitly tested for some sites (e.g., CG1, Devil's Lair, Mungo Shawcross Trench, Nawarla Gabarnmang, Riwi) using different pretreatment methods or screening, offering more robust age estimates, particularly when cross-checked with optical dating. Some samples also have calibrated ages that lie at or beyond the 55 cal ka BP limit of the SHCal20 and Marine20 curves.

Fourth, seven of the 17 sites in Fig. 12 have chronologies based on a single optical age, and with D_e estimates obtained from multi-grain, rather than single-grain, measurements. While the resulting ages may be accurate, this should ideally be demonstrated using single-grain measurements or by comparison with independent dating techniques to validate assumptions made about stratigraphic integrity and association with human occupation.

On present evidence, careful consideration of precision and context suggests that the oldest sites are in Western Australia—including the Kimberley—and in Arnhem Land in the Northern Territory. The timing of earliest use of most of these sites is imprecise, however, and their chronologies collectively form part of a broad distribution with uncertainties that statistically overlap. This limits our ability to use this evidence to resolve the timing of the first peopling of Sahul. Age estimates for initial occupation of the diverse regions of Australia—including the Kimberley, the west coast and extreme southwest corner of the continent, and the arid and semi-arid interior of Australia—all support expansion during MIS 3 (Turney et al., 2001; Hamm et al., 2016; Veth et al., 2017; McDonald et al., 2018; Jankowski et al., 2020).

To move the debate forward, an improved understanding is needed of the contextual association between the dated samples and the archaeological record. Further high-resolution dating studies, employing the systematic application of rigorous sample pretreatment and measurement procedures, coupled with statistical analyses, are required to improve the accuracy and precision with which chronologies can be constructed within individual sites and compared between sites. In the Kimberley, CG1 and Riwi are exemplars of this approach, with the latter study (Wood et al., 2016) utilising a systematic and multi-method dating strategy to provide a test of the accuracy of radiocarbon and optical ages.

7. Conclusions

The optical age of ~50 ka for the basal layer at Widgingarri 1 indicates that the site is older than previously thought. With the addition of Widgingarri 1 to the list of known Australian sites older than 46 ka, the Kimberley now has more such sites than any other region of comparable size on the continent. The occupation pattern established in the Kimberley is reflected more broadly across the northwest of the continent, which contains more than half of the earliest occupation sites in Sahul. Widgingarri 1 also contains very early examples of ground axe technology, positioning it amongst the rapidly expanding cohort of ancient Australian sites that contain precociously early examples of this technological innovation. New excavations are required, however, to obtain a more complete picture of the stratigraphy and site-formation processes at Widgingarri 1 and its occupation history. A detailed excavation and dating program would enable the construction of a high-resolution chronological framework to help interpret changes in

artefact patterns and human use of the site through time.

Author contributions

S.O'C. conducted the excavation at Widgingarri 1 and collected the artefact assemblages and radiocarbon dating samples. R.G.R. collected the optical dating samples. K.N., Z.J. and R.G.R. performed the optical dating and R.W. conducted the radiocarbon dating. C.S. analysed the stone artefacts. W.M.S. sourced the chronological data for the Kimberley and entered them into the OCTOPUS database, R.W. calibrated the radiocarbon ages and constructed the Bayesian age models, and K.N. reviewed the chronological data, sourced the archaeological data, and generated the archaeological, spatial and chronological syntheses. K.N, C.S., Z.J. and R.G.R. wrote the paper, and W.M. and P.C. reviewed and commented extensively on the manuscript. All other co-authors contributed substantially to developing the manuscript.

Declaration of competing interest

The authors declare that they have no known competing financial interests or personal relationships that could have appeared to influence the work reported in this paper.

Acknowledgements

We gratefully acknowledge the support and assistance of the elders and representatives of the Traditional Owners we consulted with who were living at One Arm Point and Mowanjum communities during the original field survey and excavation. This study was funded by the Australian Research Council through a Centre of Excellence Grant (CE170100015) to R.G.R., Z.J. and S.O'C., and an Australian Government Research Training Program Award to K.N. We thank Rebecca Esmay and Stewart Fallon for radiocarbon dating and Ulrike Troitzsch for XRD analyses. We acknowledge the support and assistance of the current Traditional Owner of the Widgingarri site, Wudugu Malanali, and the Dambimangarri Aboriginal Corporation, in reviewing and updating the results of our fieldwork. We thank the anonymous reviewers for their helpful feedback on improving this manuscript.

Appendix A. Supplementary data

Supplementary data to this article can be found online at https://doi.org/10.1016/j.quascirev.2022.107577.

References

Akerman, K., 2018. The Esoteric and Decorative Use of Bone, Shell, and Teeth in AustraliaLangley, M., Litster, M., Wright, D., May, S.K. (Eds.), In: The Archaeology of Portable Art: Southeast Asian, Pacific, and Australian Perspectives. Routledge, pp. 199–219.

Akerman, K., Fullagar, R., van Gijn, A., 2002. Weapons and wunan: production, function and exchange of Kimberley points. Aust. Aborig. Stud. (1), 13–42.

Arnold, L.J., Roberts, R.G., 2009. Stochastic modelling of multi-grain equivalent dose (De) distributions: implications for OSL dating of sediment mixtures. Quat. Geochronol. 4 (3), 204–230.

Arnold, L.J., Roberts, R.G., Galbraith, R.F., DeLong, S.B., 2009. A revised burial dose estimation procedure for optical dating of young and modern-age sediments. Quat. Geochronol. 4 (4), 306–325.

Aubert, M., 2012. A review of rock art dating in the Kimberley, Western Australia. J. Archaeol. Sci. 39 (3), 573–577.

Balme, J., O'Connor, S., Bar-Yosef Mayer, D.E., Bonsall, C., Choyke, A.M., 2017. Traditions and Change in Scaphopod Shell Beads in Northern Australia from the Pleistocene to the Recent Past. Not Just for Show: the Archaeology of Beads, Beadwork and Personal Ornaments. Oxbow Books, Oxford, pp. 7–18.

Balme, J., O'Connor, S., Maloney, T.I.M., Vannieuwenhuyse, D., Aplin, K.E.N., Dilkes-Hall, I.E., 2019. Long-term occupation on the edge of the desert: Riwi cave in the southern Kimberley, western Australia. Archaeol. Ocean. 54 (1), 35–52.

Bird, M.I., Beaman, R.J., Condie, S.A., Cooper, A., Ulm, S., Veth, P., 2018. Palaeogeography and voyage modeling indicates early human colonization of Australia was likely from Timor-Roti. Quat. Sci. Rev. 191, 431–439.

Bird, M.I., Condie, S.A., O'Connor, S., O'Grady, D., Reepmeyer, C., Ulm, S., Zega, M., Saltre, F., Bradshaw, C.J.A., 2019. Early human settlement of Sahul was not an accident. Sci. Rep. 9 (1), 1–10.

Birdsell, J.B., 1977. The Recalibration of a Paradigm for the First Peopling of Greater Australia. In: Allen, J., Golson, J., Jones, R. (Eds.), Sunda and Sahul: Prehistoric Studies in Southeast Asia, Melanesia, and Australia. Academic Press, London, pp. 113–167.

Bøtter-Jensen, L., Andersen, C., Duller, G.A., Murray, A.S., 2003. Developments in radiation, stimulation and observation facilities in luminescence measurements. Radiat. Meas. 37 (4–5), 535–541.

Bøtter-Jensen, L., Mejdahl, V., 1988. Assessment of beta dose-rate using a GM multicounter system. Int. J. Radiat. Appl. Instrum. Nucl. Tracks Radiat. Meas. 14 (1–2), 187–191.

Bowdler, S., O'Connor, S., 1991. The dating of the Australian small tool tradition, with new evidence from the Kimberley, WA. Aust. Aborig. Stud. (1), 53–62.

Bradshaw, C.J., Norman, K., Ulm, S., Williams, A.N., Clarkson, C., Chadœuf, J., Lin, S.C., Jacobs, Z., Roberts, R.G., Bird, M.I., 2021. Stochastic models support rapid peopling of Late Pleistocene Sahul. Nat. Commun. 12 (1), 1–11.

Clarkson, C., 2007. Lithics in the Land of the Lightning Brothers : the Archaeology of Wardaman Country, Northern Territory. ANU Press, Canberra ACT.

Clarkson, C., 2013. Measuring core reduction using 3D flake scar density: a test case of changing core reduction at Klasies River Mouth, South Africa. J. Archaeol. Sci. 40 (12), 4348–4357.

Clarkson, C., Jacobs, Z., Marwick, B., Fullagar, R., Wallis, L., Smith, M., Roberts, R.G., Hayes, E., Lowe, K., Carah, X., Florin, S.A., McNeil, J., Cox, D., Arnold, L.J., Hua, Q., Huntley, J., Brand, H.E.A., Manne, T., Fairbairn, A., Shulmeister, J., Lyle, L., Salinas, M., Page, M., Connell, K., Park, G., Norman, K., Murphy, T., Pardoe, C., 2017. Human occupation of northern Australia by 65,000 years ago. Nature 547 (7663), 306–310.

Cropper, D., Boone, L. (Eds.), 2018. Rockshelter Excavations in the East Hamersley Range, Pilbara Region. Oxford, Archaeopress Publishing Ltd, Western Australia.

Cupper, M.L., Duncan, J., 2006. Last glacial megafaunal death assemblage and early human occupation at Lake Menindee, southeastern Australia. Quater. Res. 66 (2), 332–341.

Codilean, A.T., Munack, H., Saktura, W.M., Cohen, T.J., Jacobs, Z., Ulm, S., Hesse, P.P., Heyman, J., Peters, K.J., Williams, A.N., Saktura, R.B.K., Rui, X., Chishiro-Dennelly, K., Panta, A., 2022. OCTOPUS Database v.2. Earth Syst. Sci. Data Discuss., Copernicus Publications 2022, 1–30.

Cohen, T.J., Saktura, W.M., Jansen, J.D., Price, D., Rui, X., Saktura, R.B., Munack, H., Codilean, A.T., 2021. OCTOPUS Database v. 2: The SahulSed Fluvial TL collection. Sahul-wide database of published sedimentary records with radiometric ages. In: ARC Centre of Excellence for Australian Biodiversity and Heritage (CABAH); University of Wollongong.

David, B., Delannoy, J.-J., Mialanes, J., Clarkson, C., Petchey, F., Geneste, J.-M., Manne, T., Bird, M.I., Barker, B., Richards, T., Chalmin, E., Castets, G., 2019. 45,610–52,160 years of site and landscape occupation at Nawarla Gabarnmang, Arnhem Land plateau (northern Australia). Quat. Sci. Rev. 215, 64–85.

Denniston, R.F., Wyrwoll, K.-H., Asmerom, Y., Polyak, V.J., Humphreys, W.F., Cugley, J., Woods, D., LaPointe, Z., Peota, J., Greaves, E., 2013. North Atlantic forcing of millennial-scale Indo-Australian monsoon dynamics during the Last Glacial period. Quat. Sci. Rev. 72, 159–168.

Dortch, C.E., Roberts, R.G., 1996. An evaluation of radiocarbon chronologies at Miriwun rock shelter and the Monsmont site, Ord valley, east Kimberley, Western Australia. Aust. Archaeol. 42 (1), 24–34.

Fallon, S., Fifield, L.K., Chappell, J., 2010. The next chapter in radiocarbon dating at the Australian National University: status report on the single stage AMS. Nucl. Instrum. Methods Phys. Res. Sect. B Beam Interact. Mater. Atoms 268 (7–8), 898–901.

Finch, D., Gleadow, A., Hergt, J., Heaney, P., Green, H., Myers, C., Veth, P., Harper, S., Ouzman, S., Levchenko, V.A., 2021. Ages for Australia's oldest rock paintings. Nat. Human Behav. 5 (3), 310–318.

Galbraith, R.F., Roberts, R.G., 2012. Statistical aspects of equivalent dose and error calculation and display in OSL dating: an overview and some recommendations. Quat. Geochronol. 11, 1–27.

Galbraith, R.F., Roberts, R.G., Laslett, G.M., Yoshida, H., Olley, J.M., 1999. Optical dating of single and multiple grains of quartz from Jinmium rock shelter, northern Australia: Part I, experimental design and statistical models. Archaeometry 41 (2), 339–364.

Green, H., Gleadow, A., Finch, D., Hergt, J., Ouzman, S., 2017. Mineral deposition systems at rock art sites, Kimberley, Northern Australia—field observations. J. Archaeol. Sci.: Report 14, 340–352.

Hamm, G., Mitchell, P., Arnold, L.J., Prideaux, G.J., Questiaux, D., Spooner, N.A., Levchenko, V.A., Foley, E.C., Worthy, T.H., Stephenson, B., Coulthard, V., Coulthard, C., Wilton, S., Johnston, D., 2016. Cultural innovation and megafauna interaction in the early settlement of arid Australia. Nature 539 (7628), 280–283.

Harrison, R., 2004. Kimberley points and colonial preference: new insights into the chronology of pressure flaked point forms from the southeast Kimberley, Western Australia. Archaeol. Ocean. 39 (1), 1–11.

Heaton, T.J., Köhler, P., Butzin, M., Bard, E., Reimer, R.W., Austin, W.E.N., Bronk Ramsey, C., Grootes, P.M., Hughen, K.A., Kromer, B., Reimer, P.J., Adkins, J., Burke, A., Cook, M.S., Olsen, J., Skinner, L.C., 2020. Marine20—the marine radiocarbon age calibration curve (0–55,000 cal BP). Radiocarbon 62 (4),

779–820.
Hiscock, P., 1994. Technological responses to risk in Holocene Australia. J. World PreHistory 8 (3), 267–292.
Hiscock, P., O'Connor, S., Balme, J., Maloney, T., 2016. World's earliest ground-edge axe production coincides with human colonisation of Australia. Aust. Archaeol. 82 (1), 2–11.
Hogg, A.G., Heaton, T.J., Hua, Q., Palmer, J.G., Turney, C.S., Southon, J., Bayliss, A., Blackwell, P.G., Boswijk, G., Ramsey, C.B., Pearson, C., Petchey, F., Reimer, P., Reimer, R., Wacker, L., 2020. SHCal20 Southern Hemisphere calibration, 0–55,000 years cal BP. Radiocarbon 62 (4), 759–778.
Huntley, D.J., Godfrey-Smith, D.I., Thewalt, M.L., 1985. Optical dating of sediments. Nature 313 (5998), 105–107.
Jacobs, Z., Roberts, R.G., 2007. Advances in optically stimulated luminescence dating of individual grains of quartz from archeological deposits. Evol. Anthropol. Issues News Rev. 16 (6), 210–223.
Jankowski, N.R., Stern, N., Lachlan, T.J., Jacobs, Z., 2020. A high-resolution late Quaternary depositional history and chronology for the southern portion of the Lake Mungo lunette, semi-arid Australia. Quat. Sci. Rev. 233.
Kealy, S., Louys, J., O'Connor, S., 2018. Least-cost pathway models indicate northern human dispersal from Sunda to Sahul. J. Hum. Evol. 125, 59–70.
Kemp, C.W., Tibby, J., Arnold, L.J., Barr, C., 2019. Australian hydroclimate during Marine Isotope Stage 3: a synthesis and review. Quat. Sci. Rev. 204, 94–104.
Langley, M.C., O'Connor, S., Aplin, K., 2016. A >46,000-year-old kangaroo bone implement from Carpenter's Gap 1 (Kimberley, northwest Australia). Quat. Sci. Rev. 154, 199–213.
Langley, M.C., Balme, J., O'Connor, S., 2021. Bone artifacts from Riwi Cave, south-central Kimberley: Reappraisal of the timing and role of osseous artifacts in northern Australia. Int. J. Osteoarchaeol. 1–10.
Maloney, T., O'Connor, S., Balme, J., 2014. New dates for point technology in the Kimberley. Archaeol. Ocean. 49 (3), 137–147.
Maloney, T., O'Connor, S., Vannieuwenhuyse, D., Balme, J., Fyfe, J., 2016. Re-excavation of Djuru, a Holocene rockshelter in the southern Kimberley, north western Australia. Aust. Archaeol. 82 (1), 80–85.
Maloney, T., O'Connor, S., Wood, R., Aplin, K., Balme, J., 2018. Carpenters Gap 1: a 47,000 year old record of indigenous adaption and innovation. Quat. Sci. Rev. 191, 204–228.
Maloney, T.R., Dilkes-Hall, I.E., 2020. Assessing the spread and uptake of tula adze technology in the late Holocene across the Southern Kimberley of Western Australia. Aust. Archaeol. 86 (3), 264–283.
Maloney, T.R., O'Connor, S., Balme, J., 2017. The effect of retouch intensity on mid to late Holocene unifacial and bifacial points from the Kimberley. Aust. Archaeol. 83 (1–2), 42–55.
Maloney, T.R., O'Connor, S., Dilkes-Hall, I.E., Langley, M.C., 2018. Late Holocene edge-ground axe production and marine shell beads from Brooking Gorge 1 rockshelter, southern Kimberley. Aust. Archaeol. 84 (2), 196–202.
McDonald, J., Reynen, W., Petchey, F., Ditchfield, K., Byrne, C., Vannieuwenhuyse, D., Leopold, M., Veth, P., 2018. Karnatukul (Serpent's Glen): a new chronology for the oldest site in Australia's Western Desert. PLoS One 13 (9), e0202511.
Moore, M.W., Westaway, K., Ross, J., Newman, K., Perston, Y., Huntley, J., Keats, S., Corporation, K.A., Morwood, M.J., 2020. Archaeology and art in context: excavations at the gunu site complex, northwest Kimberley, western Australia. PLoS One 15 (2), e0226628.
Murray, A., Roberts, R., 1998. Measurement of the equivalent dose in quartz using a regenerative-dose single-aliquot protocol. Radiat. Meas. 29 (5), 503–515.
Murray, A., Roberts, R., Wintle, A., 1997. Equivalent dose measurement using a single aliquot of quartz. Radiat. Meas. 27 (2), 171–184.
Murray, A., Wintle, A., 1998. Factors controlling the shape of the OSL decay curve in quartz. Radiat. Meas. 29 (1), 65–79.
Murray, A., Wintle, A., 1999. Isothermal decay of optically stimulated luminescence in quartz. Radiat. Meas. 30 (1), 119–125.
Murray, A.S., Wintle, A.G., 2000. Luminescence dating of quartz using an improved single-aliquot regenerative-dose protocol. Radiat. Meas. 32 (1), 57–73.
Nagle, N., Van Oven, M., Wilcox, S., van Holst Pellekaan, S., Tyler-Smith, C., Xue, Y., Ballantyne, K.N., Wilcox, L., Papac, L., Cooke, K., 2017. Aboriginal Australian mitochondrial genome variation–an increased understanding of population antiquity and diversity. Sci. Rep. 7 (1), 1–12.
Norman, K., Inglis, J., Clarkson, C., Faith, J.T., Shulmeister, J., Harris, D., 2018. An early colonisation pathway into northwest Australia 70-60,000 years ago. Quat. Sci. Rev. 180, 229–239.
O'Connor, S., 1999. 30,000 Years of Aboriginal Occupation: Kimberley, North West Australia. ANH Publications and the Centre for Archaeological Research, Australian National University, Canberra, ACT.
O'Connor, S., Aplin, K., Collins, S., 2008. A small salvage excavation in Windjana Gorge, Kimberley, western Australia. Archaeol. Ocean. 43 (2), 75–81.
O'Connor, S., Fankhauser, B.L., Anderson, A., Lilley, I., Canberra, S. O'Connor, 2001. Art at 40,000 BP? One Step Closer: an Ochre Covered Rock from Carpenter's Gap Shelter 1, Kimberley Region, Western Australia. In: Histories of Old Ages: Essays in Honour of Rhys Jones. ANU Pandanus Books, pp. 287–300.
O'Connor, S., Maloney, T., Vannieuwenhuyse, D., Balme, J., Wood, R., 2014. Occupation at carpenters gap 3, Windjana Gorge, Kimberley, western Australia. Aust. Archaeol. 78 (1), 10–23.
Olley, J.M., Murray, A., Roberts, R.G., 1996. The effects of disequilibria in the uranium and thorium decay chains on burial dose rates in fluvial sediments. Quat. Sci. Rev. 15 (7), 751–760.
Olley, J.M., Roberts, R.G., Murray, A.S., 1997. Disequilibria in the uranium decay series in sedimentary deposits at Allen's Cave, Nullarbor Plain, Australia: implications for dose rate determinations. Radiat. Meas. 27 (2), 433–443.
Olley, J.M., Roberts, R.G., Yoshida, H., Bowler, J.M., 2006. Single-grain optical dating of grave-infill associated with human burials at Lake Mungo, Australia. Quat. Sci. Rev. 25 (19–20), 2469–2474.
Pargeter, J., 2016. Lithic miniaturization in late Pleistocene southern Africa. J. Archaeol. Sci.: Report 10, 221–236.
Pargeter, J., Eren, M.I., 2017. Quantifying and comparing bipolar versus freehand flake morphologies, production currencies, and reduction energetics during lithic miniaturization. Lithic Technol. 42 (2–3), 90–108.
Pedro, N., Brucato, N., Fernandes, V., Andre, M., Saag, L., Pomat, W., Besse, C., Boland, A., Deleuze, J.F., Clarkson, C., Sudoyo, H., Metspalu, M., Stoneking, M., Cox, M.P., Leavesley, M., Pereira, L., Ricaut, F.X., 2020. Papuan mitochondrial genomes and the settlement of Sahul. J. Hum. Genet. 65 (10), 875–887.
Ramsey, C.B., 2009. Bayesian analysis of radiocarbon dates. Radiocarbon 51 (1), 337–360.
Roberts, R., Walsh, G., Murray, A., Olley, J., Jones, R., Morwood, M., Tuniz, C., Lawson, E., Macphail, M., Bowdery, D., Naumann, I., 1997. Luminescence dating of rock art and past environments using mud-wasp nests in northern Australia. Nature 387 (6634), 696–699.
Roberts, R.G., Galbraith, R., Yoshida, H., Laslett, G., Olley, J.M., 2000. Distinguishing dose populations in sediment mixtures: a test of single-grain optical dating procedures using mixtures of laboratory-dosed quartz. Radiat. Meas. 32 (5–6), 459–465.
Roberts, R.G., Jacobs, Z., Li, B., Jankowski, N.R., Cunningham, A.C., Rosenfeld, A.B., 2015. Optical dating in archaeology: thirty years in retrospect and grand challenges for the future. J. Archaeol. Sci. 56, 41–60.
Roberts, R.G., Jones, R., Spooner, N.A., Head, M.J., Murray, A.S., Smith, M.A., 1994. The human colonisation of Australia: optical dates of 53,000 and 60,000 years bracket human arrival at Deaf Adder Gorge, Northern Territory. Quat. Sci. Rev. 13 (5–7), 575–583.
Saktura, W.M., Munack, H., Codilean, A.T., Jacobs, Z., Williams, A., Ulm, S., 2021a. OCTOPUS Database v.2: The SahulArch OSL collection. Sahul-wide database of published archaeological records with radiometric ages. ARC Centre of Excellence for Australian Biodiversity and Heritage (CABAH); University of Wollongong.
Saktura, W.M., Munack, H., Codilean, A.T., Wood, R., Petchey, F., Williams, A., Ulm, S., 2021b. OCTOPUS Database v.2: The SahulArch Radiocarbon collection. Sahul-wide database of published archaeological records with radiometric ages. ARC Centre of Excellence for Australian Biodiversity and Heritage (CABAH); University of Wollongong.
Shipton, C., Clarkson, C., 2015. Flake scar density and handaxe reduction intensity. J. Archaeol. Sci.: Report 2, 169–175.
Shipton, C., Kealy, S., Mahirta, A.I., Patridina, E.P.B.G.G., O'Connor, S., 2021. Pleistocene lithic technology from alor Island articulates with the records of flores and timor across southern Wallacea. PaleoAnthropology 1–20.
Shipton, C., O'Connor, S., Jankowski, N., O'Connor-Veth, J., Maloney, T., Kealy, S., Boulanger, C., 2019. A new 44,000-year sequence from Asitau Kuru (Jerimalai), Timor-Leste, indicates long-term continuity in human behaviour. Archaeol. Anthropol. Sci. 11 (10), 5717–5741.
Storm, P., Wood, R., Stringer, C., Bartsiokas, A., de Vos, J., Aubert, M., Kinsley, L., Grün, R., 2013. U-series and radiocarbon analyses of human and faunal remains from Wajak, Indonesia. J. Hum. Evol. 64 (5), 356–365.
Stuiver, M., Polach, H.A., 1977. Discussion reporting of 14C data. Radiocarbon 19 (3), 355–363.
Turney, C.S.M., Bird, M.I., Fifield, L.K., Roberts, R.G., Smith, M., Dortch, C.E., Grün, R., Lawson, E., Ayliffe, L.K., Miller, G.H., Dortch, J., Cresswell, R.G., 2001. Early human occupation at devil's Lair, southwestern Australia 50,000 Years ago. Quater. Res. 55, 3–13.
Veth, P., Ditchfield, K., Bateman, M., Ouzman, S., Benoit, M., Motta, A.P., Lewis, D., Harper, S., Corporation, B.A., 2019. Minjiwarra: archaeological evidence of human occupation of Australia's northern Kimberley by 50,000 BP. Aust. Archaeol. 85 (2), 115–125.
Veth, P., Harper, S., Ditchfield, K., Ouzman, S., Corporation, B.A., McGrath, A., Russell, L., 2021. The Case for Continuity of Human Occupation and Rock Art Production in the Kimberley, Australia. In: The Routledge Companion to Global Indigenous History. Routledge, New York, pp. 194–220.
Veth, P., Smith, M., Bowler, J., Fitzsimmons, K., Williams, A., Hiscock, P., 2009. Excavations at parnkupirti, lake gregory, great sandy desert: OSL ages for occupation before the last glacial maximum. Aust. Archaeol. 69 (1), 1–10.
Veth, P., Ward, I., Manne, T., Ulm, S., Ditchfield, K., Dortch, J., Hook, F., Petchey, F., Hogg, A., Questiaux, D., Demuro, M., Arnold, L., Spooner, N., Levchenko, V., Skippington, J., Byrne, C., Basgall, M., Zeanah, D., Belton, D., Helmholz, P., Bajkan, S., Bailey, R., Placzek, C., Kendrick, P., 2017. Early human occupation of a maritime desert, Barrow Island, North-West Australia. Quat. Sci. Rev. 168, 19–29.
Ward, I.A.K., Fullagar, R.L.K., Boer-Mah, T., Head, L.M., Taçon, P.S.C., Mulvaney, K., 2006. Comparison of sedimentation and occupation histories inside and outside rock shelters, Keep-River region, northwestern Australia. Geoarchaeology 21 (1), 1–27.
Ward, I.A.K., Nanson, G.C., Head, L.M., Fullagar, R.L.K., Price, D.M., Fink, D., 2005. Late Quaternary landscape evolution in the Keep River region, northwestern Australia. Quat. Sci. Rev. 24 (16–17), 1906–1922.
Watchman, A., Taçon, P., Fullagar, R., Head, L., 2000. Minimum ages for pecked rock markings from Jinmium, north western Australia. Archaeol. Ocean. 35 (1), 1–10.

Whitau, R., Balme, J., O'Connor, S., Wood, R., 2017. Wood charcoal analysis at Riwi cave, Gooniyandi country, Western Australia. Quat. Int. 457, 140–154.
Whitau, R., Vannieuwenhuyse, D., Dotte-Sarout, E., Balme, J., O'Connor, S., 2018. Home is where the hearth is: anthracological and microstratigraphic analyses of Pleistocene and Holocene combustion features, Riwi cave (Kimberley, western Australia). J. Archaeol. Method Theor 25 (3), 739–776.
Williams, A.N., Ulm, S., Sapienza, T., Lewis, S., Turney, C.S., 2018. Sea-level change and demography during the last glacial termination and early Holocene across the Australian continent. Quat. Sci. Rev. 182, 144–154.
Wintle, A., Murray, A., 1997. The relationship between quartz thermoluminescence, photo-transferred thermoluminescence, and optically stimulated luminescence. Radiat. Meas. 27 (4), 611–624.
Wintle, A., Murray, A., 1998. Towards the development of a preheat procedure for OSL dating of quartz. Radiat. Meas. 29 (1), 81–94.
Wintle, A., Murray, A., 2000. Quartz OSL: effects of thermal treatment and their relevance to laboratory dating procedures. Radiat. Meas. 32 (5–6), 387–400.
Wintle, A.G., 1997. Luminescence dating: laboratory procedures and protocols. Radiat. Meas. 27 (5–6), 769–817.
Wintle, A.G., Murray, A., 1999. Luminescence sensitivity changes in quartz. Radiat. Meas. 30 (1), 107–118.
Wood, R., Jacobs, Z., Vannieuwenhuyse, D., Balme, J., O'Connor, S., Whitau, R., 2016. Towards an accurate and precise chronology for the colonization of Australia: the example of Riwi, Kimberley, western Australia. PLoS One 11 (9), e0160123.
Yuen, L.K., Littlejohn, M., Duchêne, S., Edwards, R., Bukulatjpi, S., Binks, P., Jackson, K., Davies, J., Davis, J.S., Tong, S.Y., 2019. Tracing ancient human migrations into Sahul using hepatitis B virus genomes. Mol. Biol. Evol. 36 (5), 942–954.
Zazzo, A., Saliège, J., 2011. Radiocarbon dating of biological apatites: a review. Palaeogeogr. Palaeoclimatol. Palaeoecol. 310 (1–2), 52–61.